



HAL
open science

Stable mercury concentrations of tropical tuna in the south western Pacific ocean: An 18-year monitoring study

Anais Medieu, David Point, Aurore Receveur, Olivier Gauthier, Valerie Allain, Heidi Pethybridge, Christophe E. Menkes, David P. Gillikin, Andrew T. Revill, Christopher J. Somes, et al.

► To cite this version:

Anais Medieu, David Point, Aurore Receveur, Olivier Gauthier, Valerie Allain, et al.. Stable mercury concentrations of tropical tuna in the south western Pacific ocean: An 18-year monitoring study. *Chemosphere*, 2021, 263, pp.128024. 10.1016/j.chemosphere.2020.128024 . hal-03246763

HAL Id: hal-03246763

<https://hal.science/hal-03246763>

Submitted on 5 Sep 2022

HAL is a multi-disciplinary open access archive for the deposit and dissemination of scientific research documents, whether they are published or not. The documents may come from teaching and research institutions in France or abroad, or from public or private research centers.

L'archive ouverte pluridisciplinaire **HAL**, est destinée au dépôt et à la diffusion de documents scientifiques de niveau recherche, publiés ou non, émanant des établissements d'enseignement et de recherche français ou étrangers, des laboratoires publics ou privés.



Distributed under a Creative Commons Attribution - NonCommercial 4.0 International License

17 **Abstract**

18 Global anthropogenic mercury (Hg) emissions to the atmosphere since industrialization are widely
19 considered to be responsible for a significant increase in surface ocean Hg concentrations. Still
20 unclear is how those inputs are converted into toxic methylmercury (MeHg) then transferred and
21 biomagnified in oceanic food webs. We used a unique long-term and continuous dataset to explore
22 the temporal Hg trend and variability of three tropical tuna species (yellowfin, bigeye, and skipjack)
23 from the southwestern Pacific Ocean between 2001 and 2018 (n=590). Temporal trends of muscle
24 nitrogen ($\delta^{15}\text{N}$) and carbon ($\delta^{13}\text{C}$) stable isotope ratios, amino acid (AA) $\delta^{15}\text{N}$ values and
25 oceanographic variables were also investigated to examine the potential influence of trophic,
26 biogeochemical and physical processes on the temporal variability of tuna Hg concentrations. For the
27 three species, we detected significant inter-annual variability but no significant long-term trend for
28 Hg concentrations. Inter-annual variability was related to the variability in tuna sampled lengths
29 among years and to tuna muscle $\delta^{15}\text{N}$ and $\delta^{13}\text{C}$ values. Complementary AA- and model-estimated
30 phytoplankton $\delta^{15}\text{N}$ values suggested the influence of baseline processes with enhanced tuna Hg
31 concentrations observed when dinitrogen fixers prevail, possibly fuelling baseline Hg methylation
32 and/or MeHg bioavailability at the base of the food web. Our results show that MeHg trends in top
33 predators do not necessary capture the increasing Hg concentrations suspected at the global oceanic
34 scale due to the complex and variable processes governing Hg deposition, methylation,
35 bioavailability and biomagnification. This illustrates the need for long-term standardized monitoring
36 programs of marine biota worldwide.

37 **Keywords:** methylmercury, stable isotope data, yellowfin tuna, bigeye tuna, skipjack tuna, New
38 Caledonia-Fiji region

39 **1. Introduction**

40 Mercury (Hg) is a widely distributed trace element of particular concern to human and ecosystem
41 health. Its toxicological effects are strongly dependent on the physical properties of its different
42 chemical forms (Hintelmann, 2010). Gaseous elemental Hg is emitted to the atmosphere through
43 natural (volcanism and erosion) and anthropogenic (fossil fuel combustion and artisanal gold mining)
44 processes (Pirrone et al., 2010). In open ocean regions, the dominant source of inorganic Hg (iHg) is
45 atmospheric deposition with other inputs coming from ocean margins, groundwater, benthic
46 sediments and hydrothermal vents (Selin et al., 2007). Only a fraction of iHg is naturally converted
47 into methylmercury (MeHg), the organometallic form of Hg characterised by strong neurotoxicity,
48 persistence and unique biomagnification properties in food webs. Over the past 150 years of the
49 industrial era, anthropogenic Hg use and emissions have considerably modified the natural global Hg
50 cycle (Selin et al., 2008). Models suggest that anthropogenic activities have increased atmospheric
51 Hg concentrations and have tripled the iHg content in the global ocean surface waters (Lamborg et
52 al., 2014), but with suspected sub-regional differences. In particular in the North Pacific Ocean,
53 surface water Hg concentrations have been reported to be higher in the eastern North Pacific than in
54 the western North Pacific (Sunderland et al., 2009). Most global models utilize ocean Hg data
55 collected in oceanic regions from the northern hemisphere, but questions have risen about how well
56 these models describe potential hemispherical ocean patterns with lower Hg concentrations reported
57 in the southern atmosphere (Horowitz et al., 2017).

58 Humans are exposed to MeHg primarily by the consumption of marine fish, especially of top
59 predators such as tuna (Mergler et al., 2007; Sunderland, 2007) as MeHg biomagnifies naturally in
60 marine food webs (Cai et al., 2007; Ordiano-Flores et al., 2011; 2012). Mercury concentrations in
61 tuna are known to vary geographically between ocean basins and species (Chouvelon et al., 2017;
62 Houssard et al., 2019; Kojadinovic et al., 2006; Nicklisch et al., 2017), sometimes exceeding food
63 safety guidelines (1 mg.kg⁻¹ fresh tissue) (WHO and UNEP Chemicals, 2008). Mercury

64 concentrations in organisms are governed by a complex interplay between physiological (age/length,
65 metabolism and assimilation efficiencies), ecological (foraging depth and food web structures),
66 biogeochemical (baseline in situ MeHg production and bioavailability) and physical (thermocline
67 depth and sea surface temperature) processes (Cai et al., 2007; Chouvelon et al., 2017; Choy et al.,
68 2009; Teffer et al., 2014). Recently, a spatial study from the western Pacific Ocean suggested that
69 fish length and deeper thermoclines (used as a proxy of tuna foraging habitat) were the two main
70 drivers enhancing Hg concentrations in tuna, with tuna trophic position (TP) and oceanic primary
71 production being of less importance but still influencing tuna Hg concentrations (Houssard et al.,
72 2019).

73 Despite their relatively high MeHg concentrations, tuna species are among the most popular fish
74 species consumed worldwide (FAO, 2018). In the central and western Pacific Ocean, tuna fisheries
75 accounted in 2017 for about 80% of the total Pacific Ocean catches and 54% of the global tuna catch
76 (Williams and Reid, 2018). For Pacific Island countries and territories, the large tuna resources
77 deliver great economic benefits through the sale of fishing access to distant water fishing nations and
78 employment in fish processing (Bell et al., 2011; Gillett, 2009). In terms of food and nutrition
79 security, tuna also represent a major source of proteins, essential fatty acids, vitamins and minerals
80 (Di Bella et al., 2015; Sirot et al., 2012). These species have been consequently identified as key
81 food resources for good nutrition to complement declining coastal resources in a context of high
82 levels of diabetes and obesity in this region, while taking into account their Hg content (Bell et al.,
83 2015).

84 Anticipating changes in human Hg exposure depends on our ability to capture and predict spatial and
85 temporal Hg trends in marine food webs. Only two temporal studies of tuna Hg content are available
86 to date, showing distinct results regarding Hg long-term trends. In the northern central Pacific Ocean
87 (Hawaii), Drevnick et al. (2015) suggested that Hg concentrations in yellowfin tuna (*Thunnus*
88 *albacares*) increased by at least 3.8% per year between 1971 and 2008, despite considering only

89 three sampling years. Conversely, in the North Atlantic Ocean, Lee et al. (2016) revealed a decadal
90 decline of Hg concentrations in Atlantic bluefin tuna (*T. thynnus*) of about 2.4 % between 2004 and
91 2012, suggesting potential benefits of the reduction of anthropogenic emission in North America.
92 Unfortunately, no complementary trophic ecology data were available in those two studies to discuss
93 if confounding ecological factors might contribute to the contrasted temporal trends of Hg content
94 documented worldwide.

95 Stable isotope ratios of nitrogen ($\delta^{15}\text{N}$) and carbon ($\delta^{13}\text{C}$) are widely used to examine trophic
96 ecology of marine organisms (Fry, 2006). In particular, $\delta^{13}\text{C}$ values provide information on basal
97 organic carbon sources while $\delta^{15}\text{N}$ values are used to estimate the TP of a consumer as they increase
98 predictably between prey and consumers. Therefore, $\delta^{15}\text{N}$ values are commonly used to explore Hg
99 biomagnification along trophic webs (Atwell et al., 1998; Cai et al., 2007; Teffer et al., 2014). In
100 addition to diet (i.e. trophic effects), variability of basal stable isotopic composition (i.e. baseline
101 effects) also affects consumer $\delta^{15}\text{N}$ values (Lorrain et al., 2015b). Thus, $\delta^{15}\text{N}$ values also represent a
102 potential proxy to infer baseline biological processes fuelling Hg methylation and/or net basal MeHg
103 bioavailability. To account for complex primary production dynamics influencing the isotopic
104 baseline, and produce accurate measures of a consumer's TP, amino acid compound-specific $\delta^{15}\text{N}$
105 analyses (AA-CSIA) are also used (Choy et al., 2015; Lorrain et al., 2015b). Within a consumer, the
106 $\delta^{15}\text{N}$ values of source amino acids (Sr-AA; e.g., phenylalanine and glycine) track the $\delta^{15}\text{N}$ values at
107 the base of the food web, while trophic AA (Tr-AA; e.g., glutamic acid), being enriched in ^{15}N with
108 each trophic level, provide information about a consumer's TP (Popp et al., 2007). Overall, the
109 combination of muscle stable isotope ratios and AA-CSIA is a powerful tool to investigate both Hg
110 methylation and biomagnification along food webs.

111 The specific objectives of our study were to i) investigate long-term trends of Hg concentrations in
112 tuna from the New Caledonia-Fiji sub-region in the southwestern Pacific Ocean, and to ii) identify
113 the main drivers of inter-annual variability of tuna Hg concentrations among physiological,

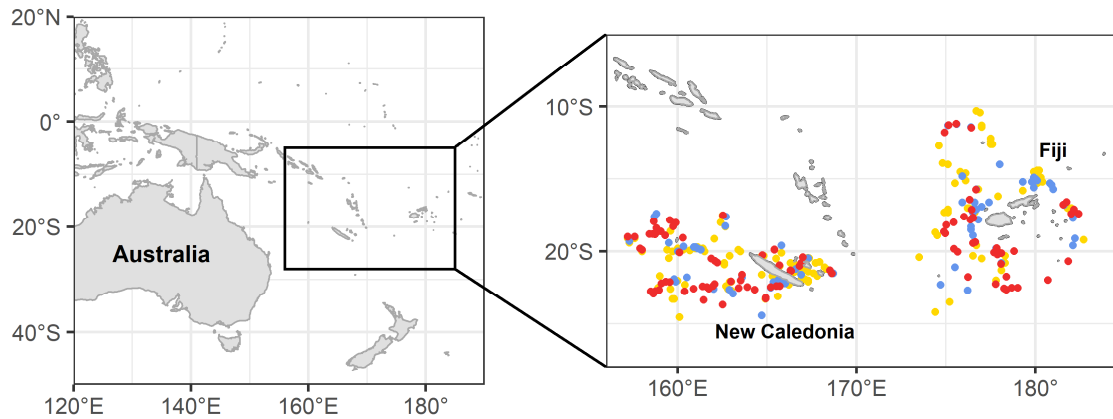
114 ecological, biogeochemical and physical parameters. We analysed a unique long-term, continuous
115 and large Hg dataset (n=590) in three commercial tropical tuna species (yellowfin, *Thunnus*
116 *albacares*; bigeye, *T. obesus*; and skipjack, *Katsuwonus pelamis*) from 2001 to 2018.
117 Complementary muscle $\delta^{15}\text{N}$ and $\delta^{13}\text{C}$ values, AA-CSIA and model estimated phytoplankton $\delta^{15}\text{N}$
118 values were also used to explore the possible influence of biogeochemical and ecological factors on
119 Hg content in tuna (i.e. changes in nutrient sources, primary productivity and tuna TP reflecting
120 pathways of energy transfer). Finally, a suite of oceanographic variables (sea surface temperature,
121 chlorophyll-a, net primary production, mixed layer depth, depths of isotherms 20°C and 12°C and
122 oceanic El Niño index) were also included as potential explanatory factors of inter-annual variability
123 in tuna Hg concentrations.

124 **2. Materials and Methods**

125 **2.1. Study area**

126 Within the large oceanic region of the south western Pacific Ocean, the New Caledonia-Fiji sub-
127 region is characterized by similar marine systems in terms of ocean dynamics, phytoplankton,
128 zooplankton, and micronekton (Le Borgne et al., 2011). Oceanographic parameters are known to be
129 driven by wind regimes, in particular southeast oriented trade winds and northwest oriented winds,
130 associated with the monsoon season. During austral summers (from December to May), the trade
131 winds become prevalent while the north-west oriented winds are more important during austral
132 winters (from May to December) (Cravatte et al., 2015; Lorrain et al., 2015a). Compared to other
133 regions in the Pacific Ocean where primary production mainly relies on NO_3^- (with particulate
134 organic matter (POM) $\delta^{15}\text{N}$ values $\sim 4\text{‰}$), our study area is known to be a hotspot of N_2 fixation
135 (POM $\delta^{15}\text{N}$ values $\sim 1\text{‰}$), with diazotrophy showing some spatial and large seasonal variability
136 (Bonnet et al., 2017; Garcia et al., 2007; Shiozaki et al., 2014). In the sub-region of New Caledonia-
137 Fiji, a significant and unique effort of collecting and archiving tuna samples has been conducted
138 since 2001 within the Pacific Marine Specimen Bank
139 (<https://www.spc.int/ofp/PacificSpecimenBank>). Previous analyses of specimens from this tissue
140 bank showed homogeneous Hg values in the New Caledonia and Fiji region (Houssard et al., 2019),
141 which justifies the consideration of this sub-region to address temporal trends. Furthermore,
142 Houssard et al. (2017) showed that tuna were relatively resident at this sub-regional scale as
143 demonstrated by the similar isotope patterns between particulate organic matter and tuna in New
144 Caledonia and Fiji.

145



146

147 Figure 1: Sample location of bigeye (blue), yellowfin (yellow), and skipjack (red) caught around New Caledonia and Fiji.

148

149 **2.2. Sample and data collection**

150 **2.2.1. Tuna sampling:** Tuna samples were taken from the Pacific Marine Specimen Bank,
 151 corresponding to 326 yellowfin, 116 bigeye and 148 skipjack tuna, spanning the 2001-2018 time
 152 period ($n_{\text{total}}=590$) (Table S1). Sampling was performed onboard commercial fishing boats (longline)
 153 by trained scientific observers from the National Observer Programs of the Pacific Island Countries
 154 and Territories. Specimens were selected from 10°S to 25°S and from 157°E to 176°W, covering the
 155 Economic Exclusive Zone (EEZ) of both New Caledonia and Fiji (Fig. 1). Fork length (FL) was
 156 measured to the lowest cm and ranged respectively for yellowfin, bigeye and skipjack from 60 to 160
 157 cm (121 ± 18 cm; mean \pm SD), 64 to 160 cm (108 ± 21 cm; mean \pm SD) and 42 to 90 cm (72 ± 7 cm;
 158 mean \pm SD). For each fish, a white muscle sample was collected from the anal area and stored frozen
 159 at -20°C prior to analyses.

160

161 **2.2.2. Environmental variables:** Seven oceanographic variables shown to influence variability of
 162 Hg concentrations in tropical tuna (Houssard et al., 2019) were used in this study to explore the
 163 physical drivers of Hg concentrations at the surface and at depth. Surface variables included monthly

164 mean sea surface temperature (SST in °C) from the National Oceanic and Atmospheric
165 Administration (NOAA, <https://www.ncdc.noaa.gov/oisst>; (Reynolds et al., 2002) and monthly
166 chlorophyll-a observations (Chl-a, mg.m⁻³) from a continuous dataset of merged L4 Ocean Colour
167 products provided by GlobColour (<http://globcolour.info>). Monthly means of net primary production
168 (NPP, mg C.m⁻².day⁻¹) were derived from a vertically generalized production model (VGPM,
169 <http://www.science.oregonstate.edu/ocean.productivity/custom.php>; Behrenfeld and Falkowski,
170 1997). Variables at depth or sub-surface included the mixed layer depth (MLD) and depths of the
171 12°C and 20°C isotherms (D_{iso12} and D_{iso20}, m), all obtained from the monthly global ARMOR3D L4
172 dataset (Guinehut et al., 2012). The Oceanic Niño Index (ONI), used to monitor the El Niño-
173 Southern Oscillation (ENSO), was also collected over the study period. Except for this last variable,
174 all monthly data were extracted on a 1° x 1° grid from 2001 to 2018. Assuming the relative oceanic
175 homogeneity of the New Caledonia-Fiji region (Houssard et al., 2017; Le Borgne et al., 2011),
176 physical variables were averaged over the entire study area to examine only temporal relationships
177 between tuna Hg concentrations and the environment. Furthermore, given the long process of MeHg
178 bioaccumulation in tuna muscle (Kwon et al., 2016), we assumed that Hg values of a given
179 individual captured at a single date and place is not exclusively explained by the environmental
180 conditions at this date, but also by the conditions prevailing during the previous months or years. As
181 ¹⁵N turnover (~six months) in tuna white muscle is known to be shorter than MeHg turnover
182 (Madigan et al., 2012), all oceanographic variables were averaged over a six-month period preceding
183 individual capture date to explain both Hg and nitrogen isotope data.

184

185 **2.2.3. Estimates of baseline phytoplankton δ¹⁵N values:** To explore the potential relationship
186 between the nitrogen cycle and change in tuna Hg concentrations at the top of the food web, baseline
187 phytoplankton δ¹⁵N values were estimated from a model of ocean biogeochemistry and isotopes
188 (MOBI, Somes et al., 2017) at each tuna sample location and year from a hindcast simulation. The

189 biogeochemical component is a 2N2PZD (2 Nutrients, 2 Phytoplankton, 1 Zooplankton, and 1
190 Detritus) ecosystem model (Somes and Oschlies, 2015). The processes in the model that fractionate
191 the nitrogen isotopes (i.e. preferentially incorporate ^{14}N into the product) are phytoplankton NO_3
192 assimilation (6 ‰), zooplankton excretion (4 ‰), N_2 fixation (1 ‰), water column denitrification
193 (20 ‰) and benthic denitrification (6 ‰), in which the respective fractionation factor yields the $\delta^{15}\text{N}$
194 difference between substrate and product (Somes et al., 2010). The baseline $\delta^{15}\text{N}$ values reproduce
195 the major features in a global seafloor $\delta^{15}\text{N}$ database (Tesdal et al., 2013).

196

197 **2.3. Analytical methods**

198 **2.3.1. Total mercury concentration analysis:** Total Hg concentrations were analysed on 590
199 samples: 326 yellowfin, 116 bigeye and 148 skipjack. The majority (n=458) of total Hg
200 concentrations were performed on homogenized freeze-dried samples by thermal decomposition,
201 gold amalgamation and atomic adsorption detection (DMA-80, Milestone, Italy) at GET (Toulouse,
202 France). Blanks and two biological standard reference materials, TORT-3 (lobster hepatopancreas;
203 $\text{Hg} = 292 \pm 22 \text{ ng.g}^{-1} \text{ dw}$) and IAEA-436 (tuna fish flesh homogenate; $\text{Hg} = 4190 \pm 360 \text{ ng.g}^{-1} \text{ dw}$),
204 covering a wide range of Hg concentrations, were routinely used in each analytical batch to check
205 Hg measurement accuracy. Complementary Hg data (n=132, only skipjack tuna) were analysed at
206 the IRD laboratory in Noumea (New Caledonia) by hot plate acidic digestion ($\text{HNO}_3\text{-H}_2\text{O}_2$) followed
207 by Cold Vapor Atomic Fluorescence Spectroscopy. Blanks and one biological standard reference
208 materials, DOMR-4 (fish protein; $\text{Hg} = 412 \pm 36 \text{ ng.g}^{-1} \text{ dw}$) were routinely used in each analytical
209 batch to check Hg measurement accuracy and traceability. Hg contents are expressed on a dry weight
210 basis (dw).

211

212 **2.3.2. Bulk muscle and compound-specific stable isotope analysis:** Muscle stable isotope ratios
213 were measured on the 590 samples analysed in Hg but also on complementary samples available
214 from our study area (n=85) but in too limited quantities to perform both Hg and stable isotope
215 analyses. In total, 675 samples were therefore analysed for stable isotopes: 360 yellowfin, 150 bigeye
216 and 165 skipjack. $\delta^{15}\text{N}$ and $\delta^{13}\text{C}$ values were obtained from ~1 mg homogenized freeze-dried
217 samples packed in tin cups and were analyzed using a Costech elemental analyser coupled to an
218 isotope ratio mass spectrometer (Thermo Scientific Delta Advantage with a Conflo IV interface) at
219 Union College (New York, USA). Reference standards (EA Consumables sorghum flour ($\delta^{13}\text{C} = -$
220 13.78 ± 0.17 , $\delta^{15}\text{N} = 1.58 \pm 0.15$), in house acetanilide ($\delta^{13}\text{C} = -34.07$, $\delta^{15}\text{N} = -0.96$), IAEA-N-2
221 ammonium sulfate ($\delta^{15}\text{N} = 20.3 \pm 0.2$), and IAEA-600 caffeine ($\delta^{13}\text{C} = -27.771 \pm 0.043$, $\delta^{15}\text{N} = 1.0 \pm$
222 0.2)) were used for isotopic corrections, and to assign the data to the appropriate isotopic scale with
223 analytical precision better than 0.1‰. Percent C and N were calculated using additional acetanilide
224 standards of varying mass. Corrections were done using a regression method. Results were reported
225 in the δ unit notation and expressed as parts per thousand (‰) relative to international standards
226 (atmospheric N_2 for nitrogen and Vienna Pee Dee belemnite (VPDB) for carbon). Reproducibility of
227 several samples measured in triplicate was <0.2 ‰. For samples with elevated lipid content (C:N >
228 3.5), $\delta^{13}\text{C}$ values were corrected using a mass balance equation with parameters derived from
229 Atlantic bluefin tuna muscle (Logan et al., 2008).

230 For AA-CSIA, we used both published (Houssard et al., 2017) and newly-analysed amino acid
231 compound-specific $\delta^{15}\text{N}$ data on yellowfin tuna (n=10) which had the most robust time series among
232 the three tuna species on individuals collected in 2003, 2007, 2010, 2013, 2016 and 2018 (n=16). To
233 do so, the freeze-dried samples were prepared by acid hydrolysis followed by esterification and
234 trifluoroacetylation as per Dale et al. (2011). The $\delta^{15}\text{N}$ isotope values of individual amino acids were
235 determined with a Trace GC gas chromatograph interfaced with a Delta V Plus isotope ratio mass
236 spectrometer (IRMS) through a GC-C combustion furnace (980°C), reduction furnace (650°C) and

237 liquid N₂ cold trap. The samples (0.5 µl) were injected splitless onto a forte BPX5 capillary column
 238 (30 m × 0.32 mm × 1.0 µm film thickness) at an injector temperature of 180°C with a constant
 239 helium flow rate of 1.5 ml min⁻¹. The column was initially held at 50°C for 2 min and then increased
 240 to 120°C at a rate of 10°C.min⁻¹. Once at 120°C, the temperature was increased at a rate of 4°C.min⁻¹
 241 to 195°C and then at 5°C.min⁻¹ to 235°C where it was held for 5 min. The temperature was then
 242 further increased to 300°C at 15°C.min⁻¹ and held for 8 min. All samples were analysed at least in
 243 triplicate. The δ¹⁵N values were normalised as follows: each sample analysis consisted of three
 244 separate IRMS analyses bracketed by a suite of amino acids with known δ¹⁵N values. The slope and
 245 intercept of known versus measured values were then used to correct the measured values for the
 246 sample set. Reproducibility associated with isotopic analysis of glutamic acid and phenylalanine
 247 averaged ± 0.44 ‰ (1 SD) and ranged from ± 0.06 ‰ to ± 0.85 ‰ respectively.

248

249 **2.3.3. Trophic position estimates:** Tuna TP was estimated using the difference of δ¹⁵N values in
 250 trophic (Tr-AA) and source (Sr-AA) amino acids, obtained by the following equation:

$$251 \quad TP_{Tr-Sr} = \frac{\delta^{15}N_{Tr-AA} - \delta^{15}N_{Sr-AA} + \beta_{Tr-Sr}}{TEF_{Tr-Sr}} + 1$$

252

253 where δ¹⁵N_{Sr-AA} is the weighted average of glycine and phenylalanine δ¹⁵N_{AA} values and
 254 δ¹⁵N_{Tr-AA} the weighted average of alanine, glutamic acid, leucine and proline δ¹⁵N_{AA} values.
 255 β_{Tr-Sr} is the difference between Tr-AA and Sr-AA in primary producers and TEF_{Tr-Sr} is the ¹⁵N
 256 enrichment between Tr-AA and Sr-AA per TP. β_{Tr-Sr} and TEF_{Tr-Sr} were set respectively at 3.6 and
 257 5.7 (Bradley et al., 2015). Using the weighted average of Sr-AA and Tr-AA reduced uncertainty due
 258 to the possible large variations of δ¹⁵N_{AA} values (Hayes et al., 1990). Uncertainty in TP estimates
 259 was calculated by propagation of errors according to Bradley et al. (2015) with a mean error of 0.4.

260 **2.4. Statistical analysis**

261 Distribution differences of Hg concentrations, muscle $\delta^{15}\text{N}$ and $\delta^{13}\text{C}$ values between species were
262 first tested with a Kruskal-Wallis test followed by Dunn's post hoc test as hypothesis of normality
263 was not met.

264

265 **2.4.1. Transformation of mercury concentrations:** Tuna Hg concentrations were log-transformed
266 to guarantee the homogeneity of variance (Zuur et al., 2010). Further, as Hg is known to
267 bioaccumulate with length (and age), a power-law relationship ($\log(\text{Hg}) = a \times (\text{FL} - b)^c - d$) was
268 fit between $\log(\text{Hg})$ and fish length (fork length, FL) to characterize the bioaccumulative processes
269 in each tuna species and remove this length effect in further analysis. This allowed the influence of
270 other potential factors governing Hg concentrations in tuna to be investigated. Residuals from the
271 length-based Hg model (i.e. observed values – predicted values) were extracted and used to calculate
272 length-standardized Hg concentrations (at mean species lengths, i.e. FL=100 cm for yellowfin and
273 bigeye and at FL=70 cm for skipjack), thereafter defined as “standardized Hg concentrations”.

274

275 **2.4.2. Temporal trend and structure analysis:** Temporal patterns of Hg concentrations in tuna
276 were examined with Moran's eigenvectors maps (MEM) which are derived from a spectral
277 decomposition of the temporal relationships among the sampling dates (Dray et al., 2006). This
278 decomposition generates orthogonal eigenfunctions that can then be used in statistical models as
279 explanatory variables representing the temporal pattern observed. Species-specific temporal
280 eigenfunction analyses were conducted on $\log(\text{Hg})$ and standardized Hg concentrations separately
281 following the method of Legendre and Gauthier (2014). To account for the seasonality in our study
282 region, each variable was aggregated by year and season, resulting in 36 season/year couples (i.e.
283 austral winter and austral summer per year from 2001 to 2018). Briefly, long-term trends of Hg

284 concentrations were first tested on seasonal means of Hg concentrations with a redundancy analysis
285 (RDA) followed by an ANOVA like permutation test. Secondly, to investigate the temporal structure
286 of log(Hg) and standardized Hg concentrations, we built distance-based matrices among the
287 sampling periods and distance-based MEMs (dbMEM) eigenfunctions. As sampling design was not
288 regular for the three tuna species, dbMEMs were built over the 36 seasons, then the seasons with no
289 sample for a species were removed as recommended with irregularly designed sampling surveys
290 (Brind'Amour et al., 2018). dbMEMs modeling positive (i.e. observations that are closer in time tend
291 to display values that are more similar than observations paired at random) or negative temporal
292 correlation between seasons were selected and tested with redundancy analysis (RDA) followed by
293 ANOVA like permutation tests to reveal any temporal structure in the response variables. Temporal
294 structure of Hg concentrations was investigated only for yellowfin and skipjack as there was not
295 enough data per season for bigeye.

296 For potential ecological and environmental drivers of Hg concentrations, only long-term trends were
297 investigated as no particular seasonal structure was revealed for both log(Hg) and standardized Hg
298 concentrations. RDA followed by ANOVA like permutation tests were then fitted separately on tuna
299 muscle $\delta^{15}\text{N}$ and $\delta^{13}\text{C}$ values, and on each environmental variable (SST, MLD, Chl-a, NPP, $D_{\text{iso}12}$
300 and $D_{\text{iso}20}$). For TP estimates and Sr-AA $\delta^{15}\text{N}$ values, as few data were available, long-term trends
301 were investigated using a linear regression fitted along years.

302

303 **2.4.3. Effects of physical and ecological drivers on the temporal variability of Hg content:**

304 Generalized additive models (GAM) were used to test the effects of potential predictors on temporal
305 variations of Hg concentrations following the formulae:

$$306 \quad Y = \alpha + s_1(X_1) + s_2(X_2) + \dots + s_n(X_n) + \varepsilon$$

307 where Y is the expected value of the response variable (i.e. $\log(\text{Hg})$ or standardized Hg
308 concentrations), α is the model intercept, $s_i(X_i)$ is a thin-plate-spline smooth function of the
309 explanatory variable i , and ε is the error term. Standardized Hg concentrations were assumed to
310 follow a Gamma distribution while $\log(\text{Hg})$ a Gaussian one. Explanatory variables tested included
311 surface (SST, Chl-a, NPP and ONI) and deep (D_{iso12} , D_{iso20} and MLD) oceanographic variables as
312 well as ecological ($\delta^{15}\text{N}$ and $\delta^{13}\text{C}$ values) factors. Fish length was also added in the models testing
313 $\log(\text{Hg})$. Before performing model computation, variance inflation factors (VIF) were calculated
314 between all explanatory variables to detect collinearity. Covariates with the highest VIF were
315 subsequently removed until the highest VIF value was < 5 (Zuur et al., 2010). With this method,
316 MLD and Chl-a were found to be collinear to other variables and were then removed from the
317 explanatory variables. D_{iso12} and D_{iso20} were highly correlated, so only separate models using either
318 D_{iso12} or D_{iso20} were tested. Explanatory variables were fitted in the GAM with a low spline
319 complexity ($k=3$) to reduce over-fitting. A backward selection approach was used and we chose the
320 model with the lowest Akaike's Information Criterion corrected for small samples sizes (AICc,
321 Burnham and Anderson, 2004). Finally, for each best-fit GAM, assumptions of residuals temporal
322 trend and auto-correlation were examined graphically with diagnostic plots. The deviance explained
323 (% DE) for each model was compared to assess predictive capacity. To determine the amount of
324 variation explained by each explanatory variable, we fitted a separate model for individual variable.
325 GAM were fitted in R using the mgcv package (Wood and Wood, 2015).

326

327 **2.4.4. Effects of baseline processes on tuna Hg concentrations and tuna $\delta^{15}\text{N}$ values:** To
328 investigate the potential influence of baseline processes, in particular the effect of different nitrogen
329 sources (NO_3^- , NO_2) fuelling primary productivity in this region (Bonnet et al., 2017; Garcia et al.,
330 2007; Shiozaki et al., 2014), we fitted linear regressions between MOBI estimates of phytoplankton
331 $\delta^{15}\text{N}$ values and both standardized Hg concentrations and muscle $\delta^{15}\text{N}$ values in the three tuna

332 species. Complementary linear regressions were fitted on yellowfin samples analysed in $\delta^{15}\text{N}$ AA-
333 CSIA to compare standardized Hg concentrations, tuna muscle $\delta^{15}\text{N}$ values and phytoplankton $\delta^{15}\text{N}$
334 estimates regarding Sr-AA $\delta^{15}\text{N}$ values, used as proxies of baseline nitrogen isotope values. All
335 statistical analyses were performed with R 3.6.1 (R Core Team, 2018).

336 **3. Results**

337 **3.1. Patterns and temporal variability of mercury concentrations**

338 Mercury concentrations (mean \pm SD, min-max, dw) differed according to species (Kruskal-Wallis,
339 $p < 0.001$) with significantly higher levels in bigeye ($2.7 \pm 1.7 \mu\text{g}\cdot\text{g}^{-1}$, 0.3-8.6 $\mu\text{g}\cdot\text{g}^{-1}$; Dunn's test,
340 $p < 0.001$) than in yellowfin ($0.7 \pm 0.5 \mu\text{g}\cdot\text{g}^{-1}$, 0.1-5.1 $\mu\text{g}\cdot\text{g}^{-1}$) and in skipjack ($0.7 \pm 0.3 \mu\text{g}\cdot\text{g}^{-1}$, 0.2-1.7
341 $\mu\text{g}\cdot\text{g}^{-1}$) (Figs. 2a & S1). Fish length and $\log(\text{Hg})$ were positively correlated and fish length explained
342 respectively 45%, 39% and 18% of the muscle Hg variations in bigeye, yellowfin and skipjack.
343 Coefficients (a, b, c and d) of the power-law relationships are specified per species in Figure 2c.

344 Inter-annual variability from 2001 to 2018 was detected in both log-transformed and standardized Hg
345 concentrations for each tuna species, yet no significant long-term temporal trends were detected
346 (Figs. 2a & 2d; Table 1). Furthermore, models based upon the MEM were not significant for any
347 variable and any tuna species (Table 1). This illustrates the lack of any significant seasonal structure
348 of $\log(\text{Hg})$ and standardized Hg concentrations between 2001 and 2018 in the south western Pacific
349 Ocean.

350

351 **3.2. Temporal variability of tuna isotopic ratios and trophic position**

352 Muscle $\delta^{15}\text{N}$ values varied between the three tuna species (Kruskal-Wallis, $p < 0.001$; Dunn's test,
353 $p < 0.001$ between all pairs of species). Highest $\delta^{15}\text{N}$ values were found in bigeye ($12.6 \pm 1.6 \text{‰}$),
354 intermediate values in yellowfin ($10.8 \pm 1.8 \text{‰}$) and lowest values in skipjack ($9.9 \pm 1.4 \text{‰}$) (Figs. 2e
355 & S1). For the three species, inter-annual variability between 2001 and 2018 was detected on muscle
356 $\delta^{15}\text{N}$ values but no increasing or decreasing long-term trends were found (Fig. 2e; Table 1).

357 Similarly, $\delta^{13}\text{C}$ values differed between species (Kruskal-Wallis, $p < 0.001$; Dunn's test, $p < 0.01$
358 between all pairs of species) with highest values in bigeye ($-16.2 \pm 1.0 \text{‰}$), intermediate values in

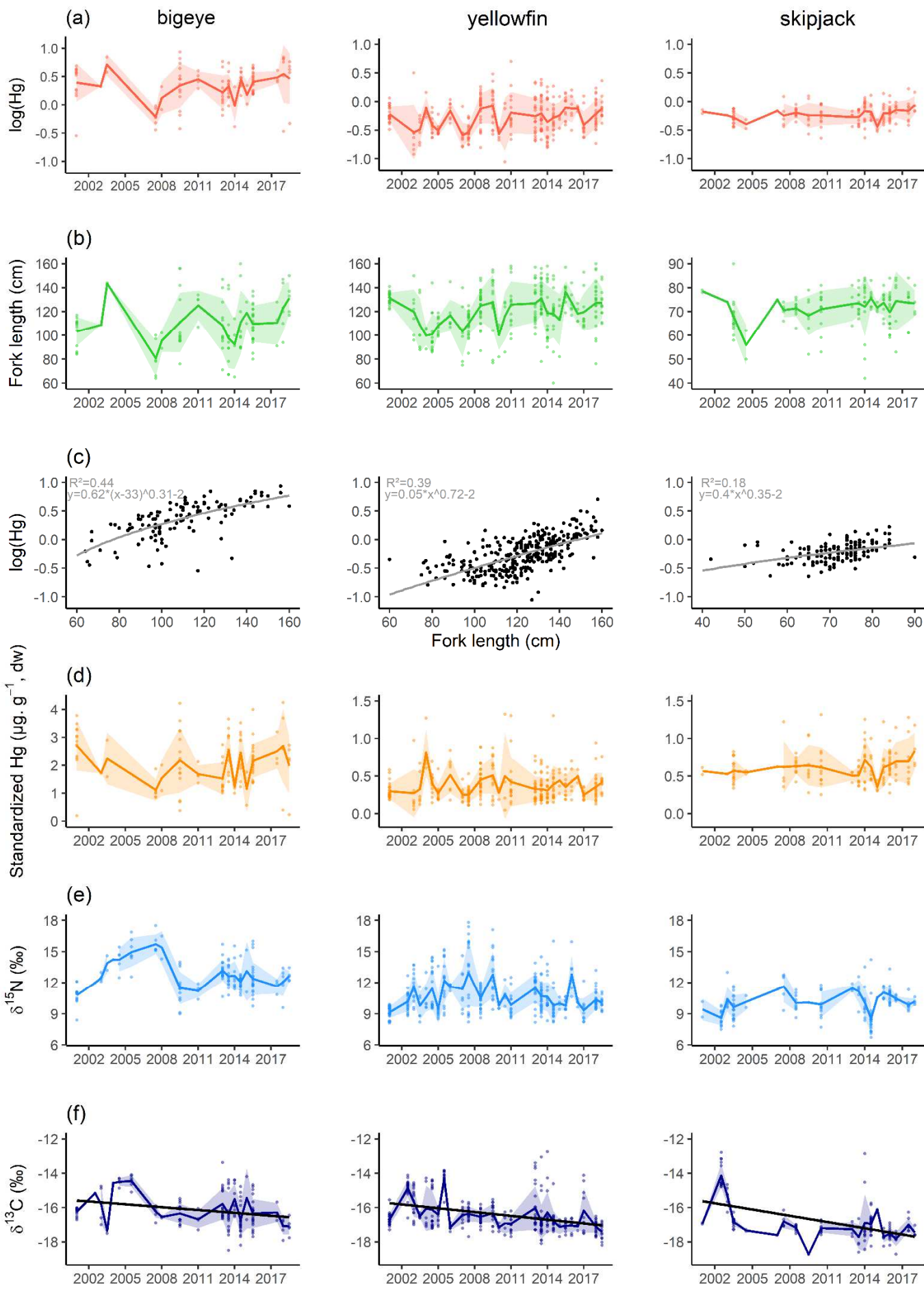
359 yellowfin ($-16.4 \pm 1.0 \text{ ‰}$) and lowest values in skipjack ($-16.8 \pm 1.1 \text{ ‰}$) (Figs 2f & S1). Contrary to
 360 muscle $\delta^{15}\text{N}$ values, $\delta^{13}\text{C}$ values were found to decrease significantly between 2001 and 2018 by a
 361 mean annual rate of 0.08 ‰ for bigeye and skipjack and of 0.07 ‰ for yellowfin (Fig. 2f; Table 1).
 362 TP estimates and Sr-AA $\delta^{15}\text{N}$ values in yellowfin varied respectively from 3.4 to 5.5 (4.5 ± 0.5) and -
 363 5.1 to 11.7 ‰ (0.4 ± 3.9) (Fig. 3). Like muscle $\delta^{15}\text{N}$ values, they varied inter-annually between 2003
 364 and 2018, however they showed no significant long-term trend ($p > 0.05$).

365

366 Table 1: ANOVA like permutation results to test temporal trend and structure of log(Hg), standardized Hg
 367 concentrations, muscle $\delta^{15}\text{N}$ values and $\delta^{13}\text{C}$ values of tropical tuna. FL: fork length; n: number of tuna individuals; *F*
 368 and *p*-value: statistics of the tests. * indicates significant temporal trend.

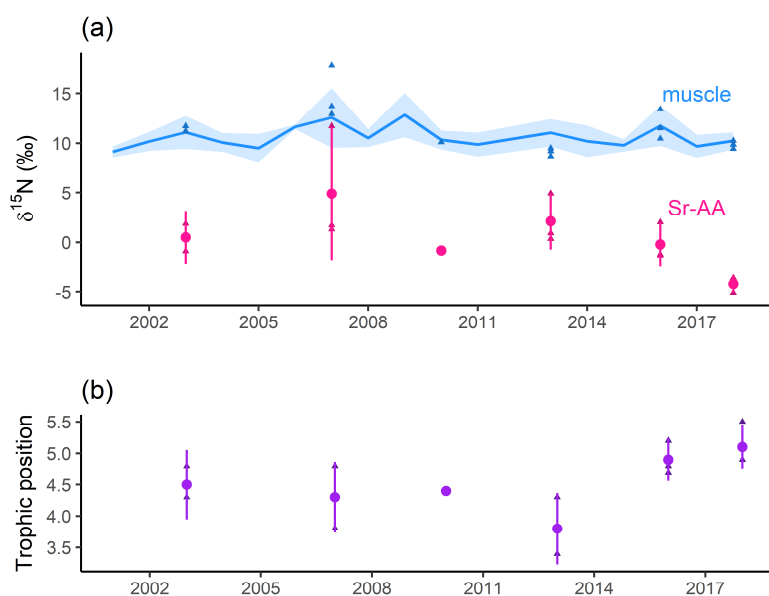
Species	Response variable	FL (cm) min-max	n	Temporal trend		MEM modelling positive correlation		MEM modelling negative correlation	
				<i>F</i>	<i>p</i> -value	<i>F</i>	<i>p</i> -value	<i>F</i>	<i>p</i> -value
bigeye	log(Hg)		116	0.088	0.800	----- Not enough data -----			
	standardized Hg	64-160	116	0.055	0.799	----- Not enough data -----			
	$\delta^{15}\text{N}$		163	0.132	0.254	----- Not tested -----			
	$\delta^{13}\text{C}$		163	4.043	0.044 *	----- Not tested -----			
yellowfin	log(Hg)		326	4.340	0.056	0.678	0.760	2.495	0.131
	standardized Hg	60-160	326	0.026	0.888	0.4903	0.887	2.15	0.202
	$\delta^{15}\text{N}$		386	0.019	0.580	----- Not tested -----			
	$\delta^{13}\text{C}$		386	10.651	0.005 *	----- Not tested -----			
skipjack	log(Hg)		148	1.470	0.247	666.170	0.053	--- Not enough data ---	
	standardized Hg	42-90	148	2.248	0.169	54.523	0.127	--- Not enough data ---	
	$\delta^{15}\text{N}$		165	1.186	0.308	----- Not tested -----			
	$\delta^{13}\text{C}$		165	4.321	0.041 *	----- Not tested -----			

369



371 Figure 2: Time series of a) log(Hg), b) tuna fork length (cm), d) standardized Hg concentrations ($\mu\text{g}\cdot\text{g}^{-1}$, dw), e) tuna
 372 muscle $\delta^{15}\text{N}$ values (‰) and f) tuna muscle $\delta^{13}\text{C}$ values (‰) (the black lines represent the significant temporal trends). c)
 373 power-law relationships between log(Hg) and fork length;. The coloured lines and shadows give respectively the
 374 seasonal means and standard deviations. The dots are the observation values.

375



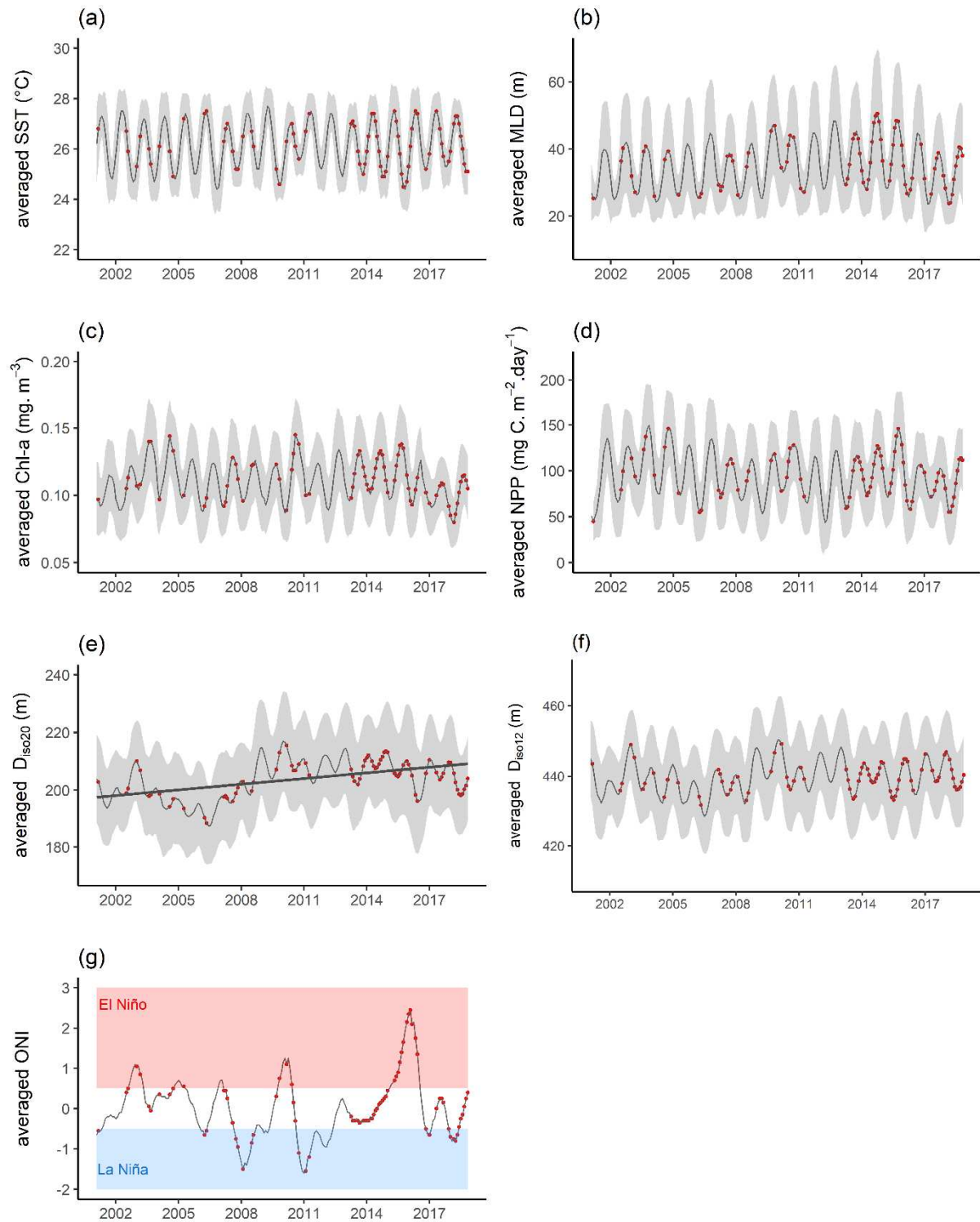
376

377 Figure 3: a) Time series of muscle $\delta^{15}\text{N}$ values (blue), source amino acid (Sr-AA) $\delta^{15}\text{N}$ values (pink) (‰) and b) trophic
 378 position (TP) estimates (purple) in yellowfin. The blue line and the blue shadow give respectively the annual means and
 379 standard deviation of muscle $\delta^{15}\text{N}$ values. The dots and lines represent respectively the mean values and the standard
 380 deviations of Sr-AA $\delta^{15}\text{N}$ values and TP estimates. The triangles are the observations for the selected yellowfin samples
 381 analysed for AA-CSIA.

382

383 3.3. Seasonal variability and trend of the environmental variables

384 Over the six environmental variables considered, only the depth of the isotherm 20°C ($D_{\text{iso}20}$) was
 385 found to increase significantly over the two last decades (Fig. 4; Table S2, $p < 0.05$). The five other
 386 variables (SST, Chl-a, MLD, NPP and $D_{\text{iso}12}$) remained stable between 2001 and 2018 (all $p > 0.05$).
 387 All physical variables showed strong seasonality over our study period.



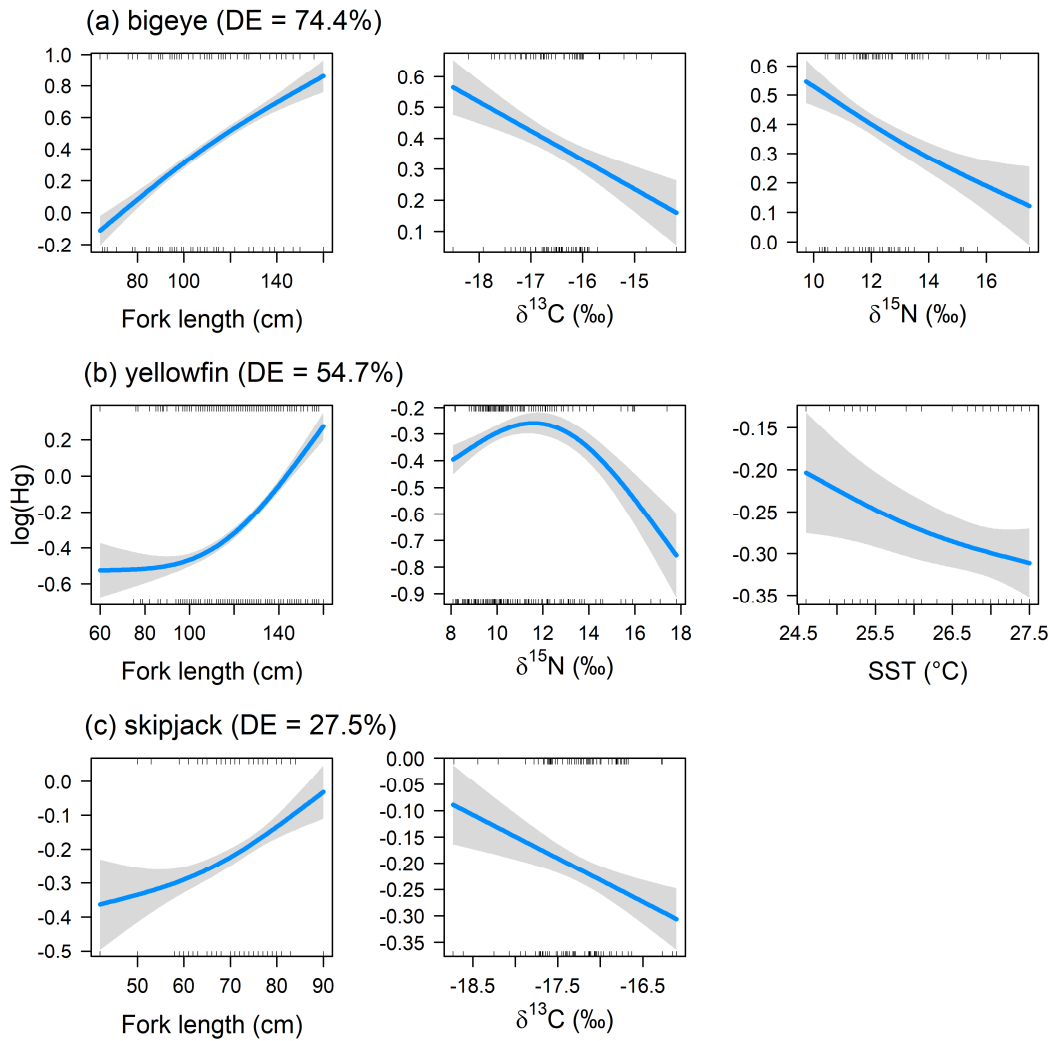
390 Figure 4: Seasonal variations of 6-month averages of oceanic variables in the New Caledonia-Fiji region. a) sea surface
 391 temperature ($^{\circ}\text{C}$), b) mixed layer depth (m), c) Chl-a ($\text{mg}\cdot\text{m}^{-3}$), d) net primary production ($\text{mg}\text{ C}\cdot\text{m}^{-2}\cdot\text{day}^{-1}$), e) depth of
 392 isotherm 20°C (m), f) depth of isotherm 12°C (m), and g) oceanic Niño index (in red: El Niño event; in blue: La Niña

393 event). The red dots represent the months with tuna samples. The grey lines and shadows give respectively the monthly
394 means and standard deviations over the 6-month period. The black regression line represents the significant temporal
395 trend.

396

397 **3.4. Drivers of the inter-annual variability of tuna Hg content**

398 For bigeye, yellowfin and skipjack respectively, the best models explained 74.4, 49.4 and 27.5 % of
399 deviance for log(Hg) and 29.3, 16 and 14.2% of deviance for standardized Hg concentrations (Table
400 2; Figs. 5 & S2). For the three species, fish length appeared as the best stand-alone predictor of
401 log(Hg), explaining 61.8, 49.4 and 21.3 % of the deviance for bigeye, yellowfin and skipjack
402 respectively. Considering standardized Hg concentrations (i.e. residuals from the length-based Hg
403 models), muscle $\delta^{15}\text{N}$ values were found to be the best stand-alone predictor of Hg distribution for
404 bigeye and yellowfin; but they were not selected in skipjack's best model. Generally, Hg
405 concentrations were found to increase with decreasing $\delta^{15}\text{N}$ values. $\delta^{13}\text{C}$ values were significant in
406 the best models of both bigeye and skipjack with lower Hg concentrations related to decreasing $\delta^{13}\text{C}$
407 values. SST was selected in the best model of yellowfin only, with response curve predicting lower
408 Hg concentrations when SST increased. No other oceanographic variables were selected in the
409 optimal models.



410

411 Figure 5: Results of the optimal generalized additive models (GAM) predicting log(Hg) in a) bigeye, b) yellowfin, and c)
 412 skipjack. The blue lines give the expected values while the grey bands show the confidence interval for the expected
 413 value. The ticks at the top and the bottom are the observed values' position associated respectively to positive and
 414 negative model residuals. DE: deviance explained.

415

416 Table 2: Results of the optimal generalized additive models (GAM) predicting log(Hg) and standardized Hg
 417 concentrations in bigeye, yellowfin and skipjack. n: number of tuna individuals; DE: deviance explained; *p*-value:
 418 statistics of the models

Species	Response variable	Explanatory variables	DE (%)	<i>p</i> -value
bigeye	log(Hg)	Length	61.8	<0.001
		$\delta^{13}\text{C}$	11.4	<0.001
		$\delta^{15}\text{N}$	10.5	<0.001

		Length + $\delta^{13}\text{C}$ + $\delta^{15}\text{N}$	74.4	
	standardized Hg	$\delta^{15}\text{N}$	17	<0.001
		$\delta^{13}\text{C}$	8.6	<0.001
		$\delta^{15}\text{N}$ + $\delta^{13}\text{C}$	29.3	
yellowfin	log(Hg)	Length	49.4	<0.001
		$\delta^{15}\text{N}$	13.2	<0.001
		SST	0.34	0.027
		Length + $\delta^{15}\text{N}$ + SST	54.7	
		$\delta^{15}\text{N}$	12.4	<0.001
	standardized Hg	SST	2.31	<0.001
		$\delta^{15}\text{N}$ + SST	16.0	
skipjack	log(Hg)	Length	21.3	<0.001
		$\delta^{13}\text{C}$	9.3	<0.001
		Length + $\delta^{13}\text{C}$	27.5	
	standardized Hg	$\delta^{13}\text{C}$	14.2	<0.001

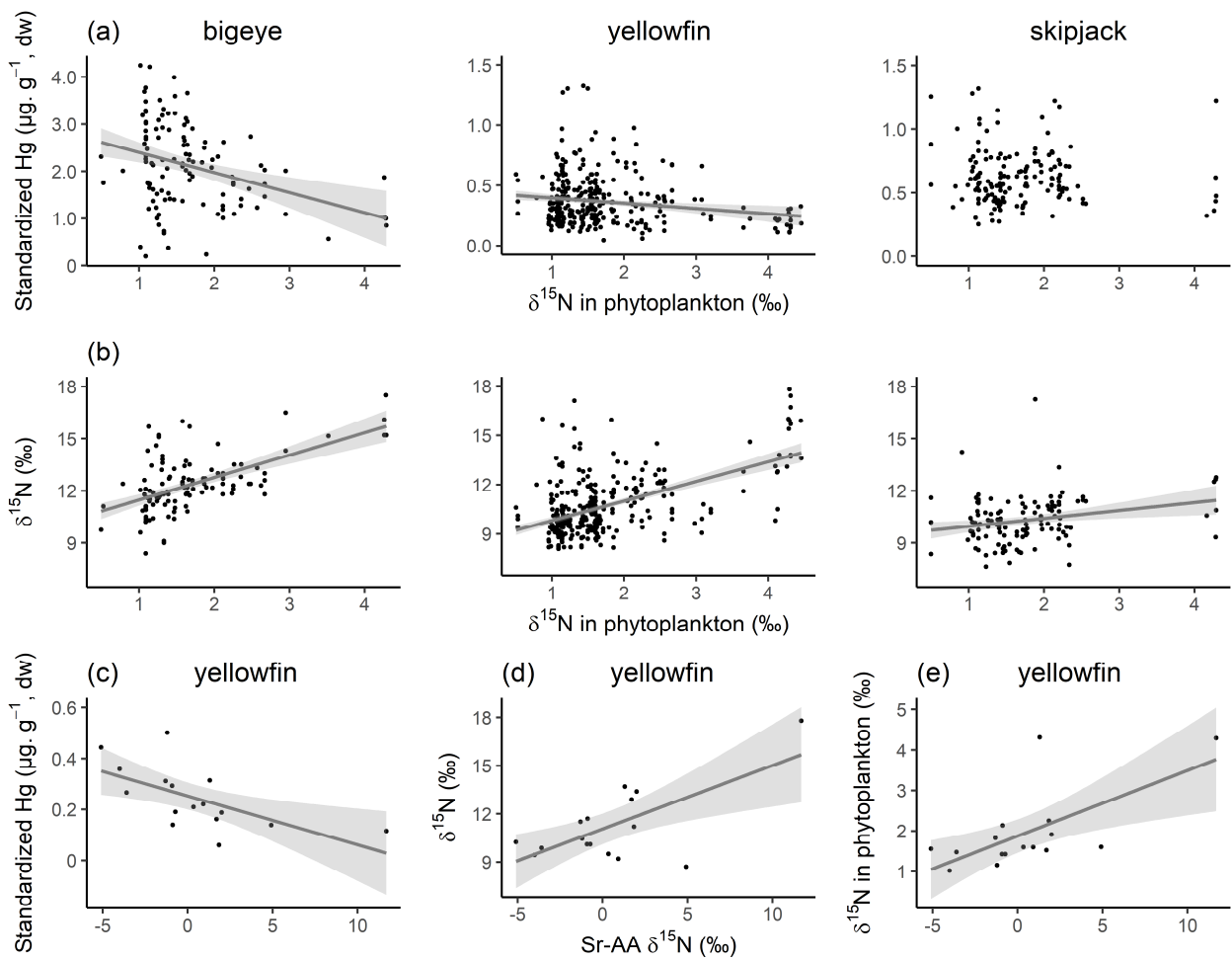
419

420

421 3.5. Mercury concentrations and tuna $\delta^{15}\text{N}$ values in relation to baseline processes

422 Standardized Hg concentrations and estimated phytoplankton $\delta^{15}\text{N}$ values were negatively correlated
423 for bigeye and yellowfin ($p < 0.05$) while no significant linear relationship was found for skipjack
424 (Fig. 6a). Conversely, tuna muscle $\delta^{15}\text{N}$ values were positively correlated to phytoplankton $\delta^{15}\text{N}$
425 estimates for the three species (Fig. 6b, $p < 0.05$). For yellowfin samples analysed in AA-CSIA,
426 standardized Hg was found to be negatively correlated to source amino acids (Sr-AA) $\delta^{15}\text{N}$ values,
427 while both tuna muscle and estimated baseline $\delta^{15}\text{N}$ values were positively correlated to Sr-AA $\delta^{15}\text{N}$
428 values (Figs. 6c, 6d & 6e, all $p < 0.05$).

429



430

431 Figure 6: Relationships between a) standardized Hg concentrations ($\mu\text{g}\cdot\text{g}^{-1}$, dw) and estimated baseline phytoplankton
 432 $\delta^{15}\text{N}$ values (‰); and b) tuna muscle $\delta^{15}\text{N}$ values (‰) and estimated baseline phytoplankton $\delta^{15}\text{N}$ values (‰). In selected
 433 yellowfin samples analysed for AA-CSIA, relationships between c) standardized Hg concentrations ($\mu\text{g}\cdot\text{g}^{-1}$, dw) and Sr-
 434 AA $\delta^{15}\text{N}$ values; d) muscle $\delta^{15}\text{N}$ values (‰) and Sr-AA $\delta^{15}\text{N}$ values (‰); and e) estimated baseline phytoplankton $\delta^{15}\text{N}$
 435 values (‰) and Sr-AA $\delta^{15}\text{N}$ (‰). The lines represent the significant linear relationships between the two variables and
 436 the grey bands show the confidence intervals.

437 **4. Discussion**

438 We report the first long-term temporal study of Hg concentrations in tropical commercial tuna from
439 the south western Pacific Ocean. Contrary to existing temporal studies of tuna Hg content in the
440 north Pacific Ocean (Hawaii, Drevnick et al., 2015) and in the north western Atlantic Ocean (Lee et
441 al., 2016), our study revealed the absence of a significant long-term trend of Hg concentrations in
442 tuna from the New Caledonia-Fiji region during the last two decades. Strong inter-annual variability
443 of Hg concentrations was however found in all three tuna species and was mainly related to the
444 variability in tuna sampled lengths among years and to biogeochemical processes occurring at the
445 primary producer level.

446

447 **4.1. Mercury concentrations in tropical tuna**

448 Among the three species, only bigeye tuna exhibited Hg concentrations exceeding the food safety
449 guideline of $1 \mu\text{g}\cdot\text{g}^{-1}$ (wet weight) (WHO and UNEP Chemicals, 2008), representing 32% of the
450 sampled specimens. Overall, most of these individuals (86 %) were bigger than 110 cm. A few
451 yellowfin were also above the food safety guideline but represented only 0.6% of the dataset. This
452 illustrates the need to consider both tuna species and fish size when addressing recommendations in
453 terms of food security regarding Hg content.

454 Relative differences of Hg concentration between the three studied tuna species in the south western
455 Pacific Ocean were similar to those reported in the north eastern and north western Pacific Ocean
456 (Blum et al., 2013; Choy et al., 2009; García-Hernández et al., 2007; Yamashita et al., 2005). The
457 highest Hg content in bigeye compared to the two other species is presumably the result of three
458 confounding factors: a higher TP for this species, a deeper vertical habitat facilitating its access to
459 mesopelagic prey with enhanced Hg concentrations, and a longer lifespan (Choy et al., 2009;
460 Houssard et al., 2019). The significant differences between species muscle $\delta^{15}\text{N}$ values could indeed

461 suggest a slightly higher TP for bigeye compared to yellowfin and skipjack, as reported in the eastern
462 Atlantic and the western Indian oceans (Sardenne et al., 2019, 2016). On the other hand, these
463 differences of $\delta^{15}\text{N}$ values could also reflect distinct foraging habitat with bigeye occupying deeper
464 habitats where prey are characterized by higher $\delta^{15}\text{N}$ values due to baseline effects (Hannides et al.,
465 2013).

466

467 **4.2. Decadal stability of tuna mercury concentrations**

468 Our study revealed no significant long-term trend of Hg concentrations between 2001 and 2018 in
469 the New Caledonia-Fiji region despite significant inter-annual variability (discussed separately
470 below). As samples were collected opportunistically onboard fishing boats, it was not possible to
471 perform our temporal analysis on the same number of samples for each species. The most complete
472 and continuous yellowfin dataset illustrates the absence of a time trend over the 18 years, and similar
473 finding applies to both skipjack and bigeye tuna.

474 Our observed stable long-term trends contrast with the estimated Hg increases of 3.8% annually
475 reported in yellowfin tuna caught near Hawaii from 1971 to 2008 (Drevnick et al., 2015) and the
476 mean annual decreasing rate of 19% from the 1990s to the early 2000s found in the Atlantic bluefin
477 tuna from the north western Atlantic Ocean (Lee et al., 2016). In this later study, the authors
478 suggested that lower Hg concentrations could be related to the reduction of anthropogenic Hg
479 emission in North America, implying a direct link between Hg anthropogenic fluctuations and tuna
480 Hg concentrations.

481 Our findings seem to confirm the fact that Hg bioaccumulation in fish do not necessarily follow the
482 global suspected increase of anthropogenic Hg emissions to the atmosphere and instead suggest
483 regional differences in oceanic Hg loads. The lack of long-term trend could be explained in part by
484 the remoteness of our region, similar to most of the south western Pacific Ocean, which has low

485 anthropogenic emissions and negligible loadings from anthropogenic sources on a total global
486 emissions scale (Horowitz et al., 2017; UN Environment, 2019). The absence of detectable decadal
487 trend in tuna Hg concentrations in this region mirrors the absence of consistent temporal trend in
488 atmospheric Hg concentrations in the southern hemisphere (Slemr et al., 2020).

489 Our contrasted results with the two other temporal studies of Hg concentrations in tuna, located in
490 the northern hemisphere, could be also related to distinct methodological approaches used to
491 investigate the temporal trend over time. Drevnick et al. (2015) performed their temporal analysis on
492 distinct, and highly heterogeneous datasets covering only three years (1971, 1998 and 2008) over a
493 long study period (37 years), and with a limited number of individuals for the most recent period
494 (n=14 in 2008). Conversely, we used a quasi-continuous long-term dataset analysed in the same
495 laboratory from 2001 to 2018 with a larger sample size and more powerful statistical tools. Finally,
496 unlike our study, no ecological proxies were available in these two other temporal studies of Hg
497 content; therefore, it was not possible to investigate the potential confounding ecological
498 contribution to the decreasing or increasing long-term trends of tuna Hg concentrations.

499

500 **4.3. Drivers of temporal variability of tuna Hg concentrations**

501 For the three tuna species, body length of sampled fish appeared to be the most important driver of
502 inter-annual variability of Hg concentrations with highest and lowest Hg concentrations in the time
503 series related to larger and smaller fish respectively (Figs. 2a, 2b & 2c). This reflects the well-known
504 bioaccumulative properties of MeHg in organisms (Adams, 2004; Cai et al., 2007; Houssard et al.,
505 2019) and is mainly related to the variability in tuna sampled sizes among years. Therefore, length-
506 standardized Hg concentrations are important to use when investigating factors governing Hg
507 bioaccumulation in tuna. This strong relationship between length and Hg content (61.8%, 49.4% and
508 21.3 % for bigeye, yellowfin and skipjack respectively) explains the relatively low scores of our

509 modelling approach for length-standardized Hg concentration as most of the variation is already
510 explained by fish length. Furthermore, for yellowfin and skipjack, where the variance of bulk Hg
511 concentrations is lower compared to bigeye, by extracting the residuals from the length-based Hg
512 models to calculate standardized Hg concentrations, we consequently reduced these variances even
513 more and therefore, the variability to be explained in our GAMs. Considering the ontogenetic dietary
514 shift in bigeye and yellowfin (Sardenne et al., 2016), fitting GAMs on distinct fish length classes
515 (e.g. small ≤ 100 cm vs large tuna > 100 cm) would have been interesting to investigate differences
516 among the main processes governing Hg methylation and MeHg bioaccumulation. Unfortunately,
517 not enough data were available to do so.

518 Considering standardized Hg concentrations (i.e. residuals from length-based Hg models), inter-
519 annual variability of Hg concentrations in bigeye and yellowfin best correlated with muscle $\delta^{15}\text{N}$
520 values, and our predictions showed generally higher Hg concentrations associated with lower muscle
521 $\delta^{15}\text{N}$ values. In the literature, most studies found that Hg is strongly correlated to organism $\delta^{15}\text{N}$
522 values, yet through a positive relationship, reflecting Hg biomagnification along the pelagic food
523 web (Cai et al., 2007; Teffer et al., 2014). Nevertheless, when exploring muscle $\delta^{15}\text{N}$ values at the
524 species level, it is important to keep in mind that they result from trophic dynamics along the food
525 web, but also from biogeochemical processes at the base of the ecosystem (baseline effects). Here,
526 muscle $\delta^{15}\text{N}$ values were positively correlated to estimated baseline phytoplankton $\delta^{15}\text{N}$ values and
527 Sr-AA $\delta^{15}\text{N}$ values, used to track baseline changes in nutrient sources and uptake. Therefore,
528 temporal variations of muscle $\delta^{15}\text{N}$ values would predominantly reflect changes at the base of the
529 food web. This could be related to the high levels of diazotrophy well documented in our study
530 region (Bonnet et al., 2017; Garcia et al., 2007; Shiozaki et al., 2014) and characterized by low POM
531 $\delta^{15}\text{N}$ values (~ 1 ‰). Atmospheric nitrogen deposition from pollution (which typically has $\delta^{15}\text{N}$
532 values ranging from -7 to 0 ‰) could also explain the low basal $\delta^{15}\text{N}$ values; yet as nitrogen
533 emissions are supposed to be low in our study area compared to the north Pacific Ocean, this

534 phenomenon is likely of less importance compared to diazotrophy (Gobel et al., 2013; Reay et al.,
535 2008). Thereby, the response curves associated with muscle $\delta^{15}\text{N}$ values (i.e. higher Hg
536 concentrations associated with lower $\delta^{15}\text{N}$ values and thus with higher diazotrophy) in our models
537 may suggest that the nitrogen cycle and/or diazotrophy (i.e. baseline effects) are likely to drive Hg
538 concentrations in the upper part of the oceanic pelagic food web, probably triggering Hg net
539 methylation and bioavailability at the base of the food web during diazotroph blooms and/or their
540 resulting remineralization. This finding is in line with the recent study by Wu et al. (2019) who
541 revealed in a meta-analysis that bioconcentration (i.e. MeHg transfer from water into the base of the
542 food web) was a better descriptor of fish MeHg concentrations than biomagnification in pelagic food
543 web. The influence of the nitrogen cycle and/or diazotrophy on Hg concentrations seems to be also
544 confirmed by the negative correlations found in this study between standardized Hg concentrations
545 and both Sr-AA $\delta^{15}\text{N}$ values and estimated baseline $\delta^{15}\text{N}$ values.

546 The community structure and growth of primary producers, as inferred by tuna $\delta^{13}\text{C}$ values, also
547 seems to influence the observed inter-annual variability of Hg concentrations, particularly for both
548 bigeye and skipjack tuna, with Hg concentrations predicted to decrease with increasing $\delta^{13}\text{C}$ values.
549 Here, $\delta^{13}\text{C}$ values were the only ecological parameter showing a significant decline between 2001
550 and 2018. The same trends were found at the global scale and were attributed to a potential global
551 shift of the phytoplankton community structure and/or physiology (Lorrain et al., 2020). The lack of
552 a corresponding long-term Hg trend in our study may suggest that the carbon cycle is likely to
553 impact Hg fate in oceans and tuna but to a lesser extent than the nitrogen cycle, and in particular
554 diazotroph blooms.

555 As dinitrogen fixers generally grow well in warm and stratified conditions, those conditions, more
556 than the nitrogen cycle itself, could be linked to the Hg cycle. Recent model predictions made on
557 Atlantic bluefin tuna show that increasing tissue Hg concentrations were related to rising seawater
558 temperatures (Schartup et al., 2019). Furthermore, experimental studies on estuarine and freshwater

559 fish have found that warmer temperatures enhanced MeHg bioaccumulation (Dijkstra et al., 2013;
560 Maulvault et al., 2016). However, here we find SST was selected in the optimal model for yellowfin
561 only, showing an opposing response curve to the above hypothesis, i.e. lower Hg concentrations in
562 tuna related to higher SST. Our response curve for yellowfin is in agreement with Houssard et al.
563 (2019) where Hg content was found to decrease spatially with increasing SST. Considering the
564 potential impact of stratification, the depth of isotherm 12°C (D_{iso12} , which can be used as a proxy of
565 the thermocline and thus stratification) was not selected in any of our optimal models. In Houssard et
566 al. (2019), D_{iso12} was found as the second main driver (after fish length) of the spatial variability of
567 tuna Hg content with Hg concentrations enhanced in regions characterised by deeper thermoclines.
568 These distinct results may suggest that the stand-alone temporal variability of the thermocline depth
569 is not responsible for the inter-annual variations of Hg concentrations in tuna muscle. While
570 discussing the impact of these environmental variables, it is worthwhile mentioning that we worked
571 at a sub-regional scale where temporal variability is low compared to large spatial variability
572 investigated in these other studies. For example, the ranges of our physical variables, especially for
573 D_{iso12} (428 – 451 m), were reduced compared to the ones investigated in Houssard et al. (2019)
574 (D_{iso12} : 200 – 460 m), which can explain their limited impact in our models.

575 Including complementary Hg data from the environment (i.e. Hg concentrations in seawater and total
576 gaseous Hg) in our modelling approach could have improved our model scores and help
577 characterizing in what extent Hg levels in tuna reflect Hg levels in water or in the atmosphere.
578 Unfortunately, such data are scarce and no time series over the two last decades were available in our
579 study area.

580

581 **4.4. Implications for global-scale monitoring of mercury in tuna**

582 With the adoption of the Minamata Convention in 2013, governments are asked to control and
583 reduce anthropogenic Hg emissions, requiring diverse ecosystem and organism studies, as well as
584 monitoring tools and strategies to track the efficiency of political decisions. Considering that tuna
585 fisheries are among the world's most important fisheries, with a commercial value estimated at 41
586 billion \$US/y in 2012 (Macfadyen, 2016), quantifying nutritional risks along with benefits are
587 becoming important when addressing food and nutritional security. Furthermore, knowing that
588 oceans have undergone large physical and biogeochemical modifications in the last decades (e.g.
589 surface warming, acidification, deoxygenation or changes in primary productivity) (Bopp et al.,
590 2013; Kwiatkowski et al., 2017), it has become necessary to assess the predictive capacity of
591 environmental variables on Hg methylation and bioaccumulation to understand potential climate-
592 driven ecological changes.

593 With a continuous and long-term dataset, we revealed for the first time the absence of significant
594 decadal trend of Hg concentrations in tropical tuna from the New Caledonia-Fiji region. This
595 contrasts with the two other available temporal studies from distinct areas (Drevnick et al., 2015; Lee
596 et al., 2016) and thus illustrates the complexity of the Hg cycle and the fact that Hg in tuna does not
597 necessarily follow the suspected recent increasing Hg trends in global oceans, especially in the
598 southern hemisphere. Our results however seem consistent with the remoteness of our study region
599 in terms of low anthropogenic emissions, and thus seem to confirm the hypothesis of distinct
600 hemispherical ocean patterns of Hg anthropogenic deposition.

601 Strong inter-annual variability was found in the three tuna species and was mainly due to fish length
602 variability among samples. This suggests the importance of using a fish length-based approach to
603 address the question of Hg spatial and temporal trends in tuna even at small (e.g. sub-regional)
604 scales. This includes accounting for different types of fishing gear (e.g. purse seine and longline)
605 employed since fishing gears are known to preferentially select certain tuna fish sizes.

606 Finally, our novel complementary investigation of baseline and trophic ecological tracers highlights
607 i) no significant decadal change in tuna TP during this 18 year period, and ii) the influence of
608 baseline processes for bigeye and yellowfin, related to the nitrogen cycle and/or diazotrophy,
609 possibly enhancing Hg methylation and/or MeHg bioavailability at the base of the food web.
610 Knowing that the largest bioaccumulation step of MeHg is likely to occur between the water
611 compartment and unicellular planktonic organisms - relative to trophic amplification processes -
612 more attention needs to be paid to ecological and physiological processes occurring at the base of
613 marine ecosystems to better capture Hg spatio-temporal trends at the top of the ocean food webs.

614 Lastly, our study emphasizes the need for more systematic collection of Hg and stable isotope data in
615 different marine reservoirs, including iHg in the water column, from both hemispheres to compare
616 MeHg production, degradation and bioaccumulation in oceans at a global scale.

617 **Declaration of competing interests**

618 The authors declare that they have no known competing financial interests or personal relationships
619 that could have appeared to influence the work reported in this paper.

620

621

622 **Acknowledgments**

623 We thank the large team of observers and supervisors from the National Observer Programs of the
624 Pacific Island Countries and Territories and FSM Arrangement Observer Program who collected the
625 tuna samples. We are grateful to the WCPFC (Western and Central Pacific Fisheries Commission)
626 Tuna Tissue Bank and the SPC (Pacific Community) Pacific Marine Specimen Bank which gave us
627 access to the tuna tissue samples. We thank the LAMA laboratory, especially Jean-Louis Duprey and
628 Stéphanie Berne for Hg analyses, as well as the Union College Stable Isotope Laboratory team
629 Anouk Verheyden, Sarah Katz, and Madelyn Miller. We also thank Pablo Brosset for his helpful
630 discussions. Funding was provided by the Pacific Fund VACOPA project and ANR-17-CE34-0010
631 MERTOX from the French Agence Nationale de la Recherche. The U.S. National Science
632 Foundation funded Union College's isotope ratio mass spectrometer and peripherals (NSF-MRI
633 #1229258).

634 **References**

- 635 Adams, D.H., 2004. Total mercury levels in tunas from offshore waters of the Florida Atlantic coast. *Marine*
636 *Pollution Bulletin* 49, 659–663. <https://doi.org/10.1016/j.marpolbul.2004.06.005>
- 637 Atwell, L., Hobson, K.A., Welch, H.E., 1998. Biomagnification and bioaccumulation of mercury in an arctic
638 marine food web: insights from stable nitrogen isotope analysis. *Can. J. Fish. Aquat. Sci.* 55, 1114–
639 1121. <https://doi.org/10.1139/f98-001>
- 640 Behrenfeld, M.J., Falkowski, P.G., 1997. Photosynthetic rates derived from satellite-based chlorophyll
641 concentration. *Limnology and Oceanography* 42, 1–20. <https://doi.org/10.4319/lo.1997.42.1.0001>
- 642 Bell, J.D., Allain, V., Allison, E.H., Andréfouët, S., Andrew, N.L., Batty, M.J., Blanc, M., Dambacher, J.M.,
643 Hampton, J., Hanich, Q., Harley, S., Lorrain, A., McCoy, M., McTurk, N., Nicol, S., Pilling, G.,
644 Point, D., Sharp, M.K., Vivili, P., Williams, P., 2015. Diversifying the use of tuna to improve food
645 security and public health in Pacific Island countries and territories. *Marine Policy* 51, 584–591.
646 <https://doi.org/10.1016/j.marpol.2014.10.005>
- 647 Bell, J.D., Reid, C., Batty, M.J., Allison, E.H., Lehodey, P., Rodwell, L., Pickering, T.D., Gillett, R., Johnson,
648 J.E., Hobday, A.J., Demmke, A., 2011. Implications of climate change for contributions by fisheries
649 and aquaculture to Pacific Island economies and communities, in: *Vulnerability of Tropical Pacific*
650 *Fisheries and Aquaculture to Climate Change: Summary for Pacific Island Countries and Territories.*
651 Secretariat of the Pacific Community, Noumea, New Caledonia, p. 71.
- 652 Blum, J.D., Popp, B.N., Drazen, J.C., Anela Choy, C., Johnson, M.W., 2013. Methylmercury production
653 below the mixed layer in the North Pacific Ocean. *Nature Geoscience* 6, 879–884.
654 <https://doi.org/10.1038/ngeo1918>
- 655 Bonnet, S., Caffin, M., Berthelot, H., Moutin, T., 2017. Hot spot of N₂ fixation in the western tropical South
656 Pacific pleads for a spatial decoupling between N₂ fixation and denitrification. *Proc Natl Acad Sci*
657 *USA* 114, E2800–E2801. <https://doi.org/10.1073/pnas.1619514114>
- 658 Bopp, L., Resplandy, L., Orr, J.C., Doney, S.C., Dunne, J.P., Gehlen, M., Halloran, P., Heinze, C., Ilyina, T.,
659 Séférian, R., Tjiputra, J., Vichi, M., 2013. Multiple stressors of ocean ecosystems in the 21st century:
660 projections with CMIP5 models. *Biogeosciences* 10, 6225–6245. [https://doi.org/10.5194/bg-10-6225-](https://doi.org/10.5194/bg-10-6225-2013)
661 [2013](https://doi.org/10.5194/bg-10-6225-2013)
- 662 Bradley, C.J., Wallsgrove, N.J., Choy, C.A., Drazen, J.C., Hetherington, E.D., Hoen, D.K., Popp, B.N., 2015.
663 Trophic position estimates of marine teleosts using amino acid compound specific isotopic analysis.
664 *Limnology and Oceanography: Methods* 13, 476–493. <https://doi.org/10.1002/lom3.10041>
- 665 Brind'Amour, A., Mahévas, S., Legendre, P., Bellanger, L., 2018. Application of Moran Eigenvector Maps
666 (MEM) to irregular sampling designs. *Spatial Statistics* 26, 56–68.
667 <https://doi.org/10.1016/j.spasta.2018.05.004>
- 668 Burnham, K.P., Anderson, D.R., 2004. Multimodel Inference: Understanding AIC and BIC in Model
669 Selection. *Sociological Methods & Research* 33, 261–304.
670 <https://doi.org/10.1177/0049124104268644>
- 671 Cai, Y., Rooker, J.R., Gill, G.A., Turner, J.P., 2007. Bioaccumulation of mercury in pelagic fishes from the
672 northern Gulf of Mexico. *Canadian Journal of Fisheries and Aquatic Sciences* 64, 458–469.
673 <https://doi.org/10.1139/f07-017>
- 674 Chauvelon, T., Brach-Papa, C., Auger, D., Bodin, N., Bruzac, S., Crochet, S., Degroote, M., Hollanda, S.J.,
675 Hubert, C., Knoery, J., Munsch, C., Puech, A., Rozuel, E., Thomas, B., West, W., Bourjea, J.,
676 Nikolic, N., 2017. Chemical contaminants (trace metals, persistent organic pollutants) in albacore tuna
677 from western Indian and south-eastern Atlantic Oceans: Trophic influence and potential as tracers of
678 populations. *Science of The Total Environment* 596–597, 481–495.
679 <https://doi.org/10.1016/j.scitotenv.2017.04.048>
- 680 Choy, C.A., Popp, B.N., Hannides, C.C.S., Drazen, J.C., 2015. Trophic structure and food resources of
681 epipelagic and mesopelagic fishes in the North Pacific Subtropical Gyre ecosystem inferred from
682 nitrogen isotopic compositions: Trophic structure of pelagic fishes. *Limnology and Oceanography* 60,
683 1156–1171. <https://doi.org/10.1002/lno.10085>

684 Choy, C.A., Popp, B.N., Kaneko, J.J., Drazen, J.C., 2009. The influence of depth on mercury levels in pelagic
685 fishes and their prey. *Proceedings of the National Academy of Sciences* 106, 13865–13869.
686 <https://doi.org/10.1073/pnas.0900711106>

687 Cravatte, S., Kestenare, E., Eldin, G., Ganachaud, A., Lefèvre, J., Marin, F., Menkes, C., Aucan, J., 2015.
688 Regional circulation around New Caledonia from two decades of observations. *Journal of Marine*
689 *Systems* 148, 249–271. <https://doi.org/10.1016/j.jmarsys.2015.03.004>

690 Dale, J., Wallsgrove, N., Popp, B., Holland, K., 2011. Nursery habitat use and foraging ecology of the brown
691 stingray *Dasyatis lata* determined from stomach contents, bulk and amino acid stable isotopes. *Mar.*
692 *Ecol. Prog. Ser.* 433, 221–236. <https://doi.org/10.3354/meps09171>

693 Di Bella, G., Potortì, A.G., Lo Turco, V., Bua, D., Licata, P., Cicero, N., Dugo, G., 2015. Trace elements in
694 *Thunnus Thynnus* from Mediterranean Sea: benefit-risk assessment for consumer. *Food Additives &*
695 *Contaminants: Part B* 8, 175–181. <https://doi.org/10.1080/19393210.2015.1030347>

696 Dijkstra, J.A., Buckman, K.L., Ward, D., Evans, D.W., Dionne, M., Chen, C.Y., 2013. Experimental and
697 Natural Warming Elevates Mercury Concentrations in Estuarine Fish. *PLoS ONE* 8, e58401.
698 <https://doi.org/10.1371/journal.pone.0058401>

699 Dray, S., Legendre, P., Peres-Neto, P.R., 2006. Spatial modelling: a comprehensive framework for principal
700 coordinate analysis of neighbour matrices (PCNM). *Ecological Modelling* 196, 483–493.
701 <https://doi.org/10.1016/j.ecolmodel.2006.02.015>

702 Drevnick, P.E., Lamborg, C.H., Horgan, M.J., 2015. Increase in mercury in Pacific yellowfin tuna: Mercury in
703 yellowfin tuna. *Environmental Toxicology and Chemistry* 34, 931–934.
704 <https://doi.org/10.1002/etc.2883>

705 FAO (Ed.), 2018. The state of world fisheries and aquaculture 2018 - Meeting the sustainable development
706 goals. Rome.

707 Fry, B., 2006. Stable isotope ecology. Springer, New York, NY.

708 Garcia, N., Raimbault, P., Sandroni, V., 2007. Seasonal nitrogen fixation and primary production in the
709 Southwest Pacific: nanoplankton diazotrophy and transfer of nitrogen to picoplankton organisms.
710 *Mar. Ecol. Prog. Ser.* 343, 25–33. <https://doi.org/10.3354/meps06882>

711 García-Hernández, J., Cadena-Cárdenas, L., Betancourt-Lozano, M., García-De-La-Parra, L.M., García-Rico,
712 L., Márquez-Farías, F., 2007. Total mercury content found in edible tissues of top predator fish from
713 the Gulf of California, Mexico. *Toxicological & Environmental Chemistry* 89, 507–522.
714 <https://doi.org/10.1080/02772240601165594>

715 Gillett, R., 2009. Fisheries in the Economies of the Pacific Island Countries and Territories. Asian
716 Development Bank.

717 Gobel, A.R., Altieri, K.E., Peters, A.J., Hastings, M.G., Sigman, D.M., 2013. Insights into anthropogenic
718 nitrogen deposition to the North Atlantic investigated using the isotopic composition of aerosol and
719 rainwater nitrate: NITRATE ISOTOPES IN MARINE AEROSOLS. *Geophys. Res. Lett.* 40, 5977–
720 5982. <https://doi.org/10.1002/2013GL058167>

721 Guinehut, S., Dhomps, A.-L., Larnicol, G., Traon, P.-Y.L., 2012. High resolution 3-D temperature and salinity
722 fields derived from in situ and satellite observations. *Ocean Science* 8, 845–857.
723 <https://doi.org/10.5194/os-8-845-2012>

724 Hannides, C.C.S., Popp, B.N., Choy, C.A., Drazen, J.C., 2013. Midwater zooplankton and suspended particle
725 dynamics in the North Pacific Subtropical Gyre: A stable isotope perspective. *Limnology and*
726 *Oceanography* 58, 1931–1946. <https://doi.org/10.4319/lo.2013.58.6.1931>

727 Hayes, J.M., Freeman, K.H., Popp, B.N., Hoham, C.H., 1990. Compound-specific isotopic analyses: A novel
728 tool for reconstruction of ancient biogeochemical processes. *Organic Geochemistry, Proceedings of*
729 *the 14th International Meeting on Organic Geochemistry* 16, 1115–1128.
730 [https://doi.org/10.1016/0146-6380\(90\)90147-R](https://doi.org/10.1016/0146-6380(90)90147-R)

731 Hintelmann, H., 2010. Organomercurials. Their Formation and Pathways in the Environment, in:
732 *Organometallics in Environment and Toxicology: Metal Ions in Life Sciences*. pp. 365–401.
733 <https://doi.org/10.1039/9781849730822-00365>

734 Horowitz, H.M., Jacob, D.J., Zhang, Y., Dibble, T.S., Slemr, F., Amos, H.M., Schmidt, J.A., Corbitt, E.S.,
735 Marais, E.A., Sunderland, E.M., 2017. A new mechanism for atmospheric mercury redox chemistry:
736 implications for the global mercury budget. *Atmospheric Chemistry and Physics* 17.
737 <https://doi.org/10.5194/acp-17-6353-2017>

- 738 Houssard, P., Lorrain, A., Tremblay-Boyer, L., Allain, V., Graham, B.S., Menkes, C.E., Pethybridge, H.,
739 Couturier, L.I.E., Point, D., Leroy, B., Receveur, A., Hunt, B.P.V., Vourey, E., Bonnet, S., Rodier,
740 M., Raimbault, P., Feunteun, E., Kuhnert, P.M., Munaron, J.-M., Lebreton, B., Otake, T., Letourneur,
741 Y., 2017. Trophic position increases with thermocline depth in yellowfin and bigeye tuna across the
742 Western and Central Pacific Ocean. *Progress in Oceanography* 154, 49–63.
743 <https://doi.org/10.1016/j.pocean.2017.04.008>
- 744 Houssard, P., Point, D., Tremblay-Boyer, L., Allain, V., Pethybridge, H., Masbou, J., Ferriss, B.E., Baya,
745 P.A., Lagane, C., Menkes, C.E., Letourneur, Y., Lorrain, A., 2019. A Model of Mercury Distribution
746 in Tuna from the Western and Central Pacific Ocean: Influence of Physiology, Ecology and
747 Environmental Factors. *Environmental Science & Technology* 53, 1422–1431.
748 <https://doi.org/10.1021/acs.est.8b06058>
- 749 Kojadinovic, J., Potier, M., Le Corre, M., Cosson, R.P., Bustamante, P., 2006. Mercury content in commercial
750 pelagic fish and its risk assessment in the Western Indian Ocean. *Science of The Total Environment*
751 366, 688–700. <https://doi.org/10.1016/j.scitotenv.2006.02.006>
- 752 Kwiatkowski, L., Bopp, L., Aumont, O., Ciais, P., Cox, P.M., Laufkötter, C., Li, Y., Séférian, R., 2017.
753 Emergent constraints on projections of declining primary production in the tropical oceans. *Nature*
754 *Clim Change* 7, 355–358. <https://doi.org/10.1038/nclimate3265>
- 755 Kwon, S.Y., Blum, J.D., Madigan, D.J., Block, B.A., Popp, B.N., 2016. Quantifying mercury isotope
756 dynamics in captive Pacific bluefin tuna (*Thunnus orientalis*). *Elem Sci Anth* 4, 000088.
757 <https://doi.org/10.12952/journal.elementa.000088>
- 758 Lamborg, C.H., Hammerschmidt, C.R., Bowman, K.L., Swarr, G.J., Munson, K.M., Ohnemus, D.C., Lam,
759 P.J., Heimbürger, L.-E., Rijkenberg, M.J.A., Saito, M.A., 2014. A global ocean inventory of
760 anthropogenic mercury based on water column measurements. *Nature* 512, 65–68.
761 <https://doi.org/10.1038/nature13563>
- 762 Le Borgne, R., Allain, V., Griffiths, S.P., Matear, R.J., McKinnon, A.D., Richardson, A.J., Young, J.W.,
763 2011. Vulnerability of open ocean food webs in the tropical Pacific to climate change, in:
764 *Vulnerability of Tropical Pacific Fisheries and Aquaculture to Climate Change*. Secretariat of the
765 Pacific Community, New Caledonia, pp. 189–249.
- 766 Lee, C.-S., Lutcavage, M.E., Chandler, E., Madigan, D.J., Cerrato, R.M., Fisher, N.S., 2016. Declining
767 Mercury Concentrations in Bluefin Tuna Reflect Reduced Emissions to the North Atlantic Ocean.
768 *Environmental Science & Technology* 50, 12825–12830. <https://doi.org/10.1021/acs.est.6b04328>
- 769 Legendre, P., Gauthier, O., 2014. Statistical methods for temporal and space-time analysis of community
770 composition data. *Proceedings of the Royal Society B: Biological Sciences* 281, 20132728–
771 20132728. <https://doi.org/10.1098/rspb.2013.2728>
- 772 Logan, J.M., Jardine, T.D., Miller, T.J., Bunn, S.E., Cunjak, R.A., Lutcavage, M.E., 2008. Lipid corrections in
773 carbon and nitrogen stable isotope analyses: comparison of chemical extraction and modelling
774 methods. *Journal of Animal Ecology* 77, 838–846. <https://doi.org/10.1111/j.1365-2656.2008.01394.x>
- 775 Lorrain, A., Clavier, J., Thébault, J., Tremblay-Boyer, L., Houllbrèque, F., Amice, E., Le Goff, M., Chauvaud,
776 L., 2015a. Variability in diel and seasonal in situ metabolism of the tropical gastropod *Tectus*
777 *niloticus*. *Aquat. Biol.* 23, 167–182. <https://doi.org/10.3354/ab00618>
- 778 Lorrain, A., Graham, B.S., Popp, B.N., Allain, V., Olson, R.J., Hunt, B.P.V., Potier, M., Fry, B., Galván-
779 Magaña, F., Menkes, C.E.R., Kaehler, S., Ménard, F., 2015b. Nitrogen isotopic baselines and
780 implications for estimating foraging habitat and trophic position of yellowfin tuna in the Indian and
781 Pacific Oceans. *Deep Sea Research Part II: Topical Studies in Oceanography* 113, 188–198.
782 <https://doi.org/10.1016/j.dsr2.2014.02.003>
- 783 Lorrain, A., Pethybridge, H., Cassar, N., Receveur, A., Allain, V., Bodin, N., Bopp, L., Choy, C.A., Duffy, L.,
784 Fry, B., Goñi, N., Graham, B.S., Hobday, A.J., Logan, J.M., Ménard, F., Menkes, C.E., Olson, R.J.,
785 Pagendam, D.E., Point, D., Reville, A.T., Somes, C.J., Young, J.W., 2020. Trends in tuna carbon
786 isotopes suggest global changes in pelagic phytoplankton communities. *Glob Change Biol* 26, 458–
787 470. <https://doi.org/10.1111/gcb.14858>
- 788 Macfadyen, G., 2016. Study of the global estimate of the value of tuna fisheries - Phase 3 Report. Poseidon
789 Aquatic Resource Management Ltd.
- 790 Madigan, D.J., Litvin, S.Y., Popp, B.N., Carlisle, A.B., Farwell, C.J., Block, B.A., 2012. Tissue Turnover
791 Rates and Isotopic Trophic Discrimination Factors in the Endothermic Teleost, Pacific Bluefin Tuna
792 (*Thunnus orientalis*). *PLOS ONE* 7, e49220. <https://doi.org/10.1371/journal.pone.0049220>

793 Maulvault, A.L., Custódio, A., Anacleto, P., Repolho, T., Pousão, P., Nunes, M.L., Diniz, M., Rosa, R.,
794 Marques, A., 2016. Bioaccumulation and elimination of mercury in juvenile seabass (*Dicentrarchus*
795 *labrax*) in a warmer environment. *Environmental Research* 149, 77–85.
796 <https://doi.org/10.1016/j.envres.2016.04.035>

797 Mergler, D., Anderson, H.A., Chan, L.H.M., Mahaffey, K.R., Murray, M., Sakamoto, M., Stern, A.H., 2007.
798 Methylmercury Exposure and Health Effects in Humans: A Worldwide Concern. *AMBIO: A Journal*
799 *of the Human Environment* 36, 3–11. [https://doi.org/10.1579/0044-](https://doi.org/10.1579/0044-7447(2007)36[3:MEAHEI]2.0.CO;2)
800 [7447\(2007\)36\[3:MEAHEI\]2.0.CO;2](https://doi.org/10.1579/0044-7447(2007)36[3:MEAHEI]2.0.CO;2)

801 Nicklisch, S.C.T., Bonito, L.T., Sandin, S., Hamdoun, A., 2017. Mercury levels of yellowfin tuna (*Thunnus*
802 *albacares*) are associated with capture location. *Environmental Pollution* 229, 87–93.
803 <https://doi.org/10.1016/j.envpol.2017.05.070>

804 Ordiano-Flores, A., Galván-Magaña, F., Rosiles-Martínez, R., 2011. Bioaccumulation of Mercury in Muscle
805 Tissue of Yellowfin Tuna, *Thunnus albacares*, of the Eastern Pacific Ocean. *Biological Trace Element*
806 *Research* 144, 606–620. <https://doi.org/10.1007/s12011-011-9136-4>

807 Ordiano-Flores, A., Rosiles-Martínez, R., Galván-Magaña, F., 2012. Biomagnification of mercury and its
808 antagonistic interaction with selenium in yellowfin tuna *Thunnus albacares* in the trophic web of Baja
809 California Sur, Mexico. *Ecotoxicology and Environmental Safety* 86, 182–187.
810 <https://doi.org/10.1016/j.ecoenv.2012.09.014>

811 Pirrone, N., Cinnirella, S., Feng, X., Finkelman, R.B., Friedli, H.R., Leaner, J., Mason, R., Mukherjee, A.B.,
812 Stracher, G.B., Streets, D.G., Telmer, K., 2010. Global mercury emissions to the atmosphere from
813 anthropogenic and natural sources. *Atmos. Chem. Phys.* 10, 5951–5964. [https://doi.org/10.5194/acp-](https://doi.org/10.5194/acp-10-5951-2010)
814 [10-5951-2010](https://doi.org/10.5194/acp-10-5951-2010)

815 Popp, B.N., Graham, B.S., Olson, R.J., Hannides, C.C.S., Lott, M.J., López-Ibarra, G.A., Galván-Magaña, F.,
816 Fry, B., 2007. Insight into the Trophic Ecology of Yellowfin Tuna, *Thunnus albacares*, from
817 Compound-Specific Nitrogen Isotope Analysis of Proteinaceous Amino Acids. *Terrestrial Ecology* 1,
818 173–190.

819 R Core Team, 2018. R: A language and environment for statistical computing; 2015. Vienna, Austria.

820 Reay, D.S., Dentener, F., Smith, P., Grace, J., Feely, R.A., 2008. Global nitrogen deposition and carbon sinks.
821 *Nature Geosci* 1, 430–437. <https://doi.org/10.1038/ngeo230>

822 Reynolds, R.W., Rayner, N.A., Smith, T.M., Stokes, D.C., Wang, W., 2002. An Improved In Situ and Satellite
823 SST Analysis for Climate. *J. Climate* 15, 1609–1625. [https://doi.org/10.1175/1520-](https://doi.org/10.1175/1520-0442(2002)015<1609:AIISAS>2.0.CO;2)
824 [0442\(2002\)015<1609:AIISAS>2.0.CO;2](https://doi.org/10.1175/1520-0442(2002)015<1609:AIISAS>2.0.CO;2)

825 Sardenne, F., Bodin, N., Chassot, E., Amiel, A., Fouché, E., Degroote, M., Hollanda, S., Pethybridge, H.,
826 Lebreton, B., Guillou, G., Ménard, F., 2016. Trophic niches of sympatric tropical tuna in the Western
827 Indian Ocean inferred by stable isotopes and neutral fatty acids. *Progress in Oceanography* 146, 75–
828 88. <https://doi.org/10.1016/j.pocean.2016.06.001>

829 Sardenne, F., Diaha, N.C., Amandé, M.J., Zudaire, I., Couturier, L.I.E., Metral, L., Le Grand, F., Bodin, N.,
830 2019. Seasonal habitat and length influence on the trophic niche of co-occurring tropical tunas in the
831 eastern Atlantic Ocean. *Canadian Journal of Fisheries and Aquatic Sciences* 76, 69–80.
832 <https://doi.org/10.1139/cjfas-2017-0368>

833 Schartup, A.T., Thackray, C.P., Qureshi, A., Dassuncao, C., Gillespie, K., Hanke, A., Sunderland, E.M., 2019.
834 Climate change and overfishing increase neurotoxicant in marine predators. *Nature* 1–3.
835 <https://doi.org/10.1038/s41586-019-1468-9>

836 Selin, N.E., Jacob, D.J., Park, R.J., Yantosca, R.M., Strode, S., Jaeglé, L., Jaffe, D., 2007. Chemical cycling
837 and deposition of atmospheric mercury: Global constraints from observations. *Journal of Geophysical*
838 *Research* 112. <https://doi.org/10.1029/2006JD007450>

839 Selin, N.E., Jacob, D.J., Yantosca, R.M., Strode, S., Jaeglé, L., Sunderland, E.M., 2008. Global 3-D land-
840 ocean-atmosphere model for mercury: Present-day versus preindustrial cycles and anthropogenic
841 enrichment factors for deposition. *Global Biogeochemical Cycles* 22, 13.
842 <https://doi.org/10.1029/2007GB003040>

843 Shiozaki, T., Kodama, T., Furuya, K., 2014. Large-scale impact of the island mass effect through nitrogen
844 fixation in the western South Pacific Ocean. *Geophysical Research Letters* 41, 2907–2913.
845 <https://doi.org/10.1002/2014GL059835>

846 Sirot, V., Leblanc, J.-C., Margaritis, I., 2012. A risk–benefit analysis approach to seafood intake to determine
847 optimal consumption. *Br J Nutr* 107, 1812–1822. <https://doi.org/10.1017/S0007114511005010>

848 Slemr, F., Martin, L., Labuschagne, C., Mkololo, T., Angot, H., Magand, O., Dommergue, A., Garat, P.,
849 Ramonet, M., Bieser, J., 2020. Atmospheric mercury in the Southern Hemisphere – Part 1: Trend and
850 inter-annual variations in atmospheric mercury at Cape Point, South Africa, in 2007–2017, and on
851 Amsterdam Island in 2012–2017. *Atmos. Chem. Phys.* 20, 7683–7692. [https://doi.org/10.5194/acp-](https://doi.org/10.5194/acp-20-7683-2020)
852 [20-7683-2020](https://doi.org/10.5194/acp-20-7683-2020)

853 Somes, C.J., Oschlies, A., 2015. On the influence of “non-Redfield” dissolved organic nutrient dynamics on
854 the spatial distribution of N₂ fixation and the size of the marine fixed nitrogen inventory. *Global*
855 *Biogeochemical Cycles* 29, 973–993. <https://doi.org/10.1002/2014GB005050>

856 Somes, C.J., Schmittner, A., Galbraith, E.D., Lehmann, M.F., Altabet, M.A., Montoya, J.P., Letelier, R.M.,
857 Mix, A.C., Bourbonnais, A., Eby, M., 2010. Simulating the global distribution of nitrogen isotopes in
858 the ocean. *Global Biogeochem. Cycles* 24, n/a-n/a. <https://doi.org/10.1029/2009GB003767>

859 Somes, C.J., Schmittner, A., Muglia, J., Oschlies, A., 2017. A Three-Dimensional Model of the Marine
860 Nitrogen Cycle during the Last Glacial Maximum Constrained by Sedimentary Isotopes. *Frontiers in*
861 *Marine Science* 4. <https://doi.org/10.3389/fmars.2017.00108>

862 Sunderland, E.M., 2007. Mercury Exposure from Domestic and Imported Estuarine and Marine Fish in the
863 U.S. Seafood Market. *Environmental Health Perspectives* 115, 235–242.
864 <https://doi.org/10.1289/ehp.9377>

865 Sunderland, E.M., Krabbenhoft, D.P., Moreau, J.W., Strobe, S.A., Landing, W.M., 2009. Mercury sources,
866 distribution, and bioavailability in the North Pacific Ocean: Insights from data and models. *Global*
867 *Biogeochemical Cycles* 23, 14. <https://doi.org/10.1029/2008GB003425>

868 Teffer, A.K., Staudinger, M.D., Taylor, D.L., Juanes, F., 2014. Trophic influences on mercury accumulation
869 in top pelagic predators from offshore New England waters of the northwest Atlantic Ocean. *Marine*
870 *Environmental Research* 101, 124–134. <https://doi.org/10.1016/j.marenvres.2014.09.008>

871 Tesdal, J.-E., Galbraith, E.D., Kienast, M., 2013. Nitrogen isotopes in bulk marine sediment: linking seafloor
872 observations with subseafloor records. *Biogeosciences* 10, 101–118. [https://doi.org/10.5194/bg-10-](https://doi.org/10.5194/bg-10-101-2013)
873 [101-2013](https://doi.org/10.5194/bg-10-101-2013)

874 UN Environment, 2019. Global mercury assessment 2018.

875 Williams, P., Reid, C., 2018. Overview of tuna fisheries in the WCPO including economic conditions - 2017.
876 Presented at the WCPFC - TCC14 - 2018, Majuro, Republic of Marshall Islands, p. 68.

877 Wood, S., Wood, M.S., 2015. Package “mgcv”. R package version (No. 1.8-28).

878 World Health Organization, UNEP Chemicals, 2008. Guidance for identifying populations at risk from
879 mercury exposure. UNEP DTIE Chemicals Branch and WHO Department of Food Safety, Zoonoses
880 and Foodborne Diseases, Geneva, Switzerland.

881 Wu, P., Kainz, M.J., Bravo, A.G., Åkerblom, S., Sonesten, L., Bishop, K., 2019. The importance of
882 bioconcentration into the pelagic food web base for methylmercury biomagnification: A meta-
883 analysis. *Science of The Total Environment* 646, 357–367.
884 <https://doi.org/10.1016/j.scitotenv.2018.07.328>

885 Yamashita, Y., Omura, Y., Okazaki, E., 2005. Total mercury and methylmercury levels in commercially
886 important fishes in Japan. *Fisheries Science* 71, 1029–1035. [https://doi.org/10.1111/j.1444-](https://doi.org/10.1111/j.1444-2906.2005.01060.x)
887 [2906.2005.01060.x](https://doi.org/10.1111/j.1444-2906.2005.01060.x)

888 Zuur, A.F., Ieno, E.N., Elphick, C.S., 2010. A protocol for data exploration to avoid common statistical
889 problems: Data exploration. *Methods in Ecology and Evolution* 1, 3–14.
890 <https://doi.org/10.1111/j.2041-210X.2009.00001.x>

891

Graphical abstract

